# Z-ENGINE PISTON FEA

## 1) Engine characteristics:

- Bore/stroke: 80/80
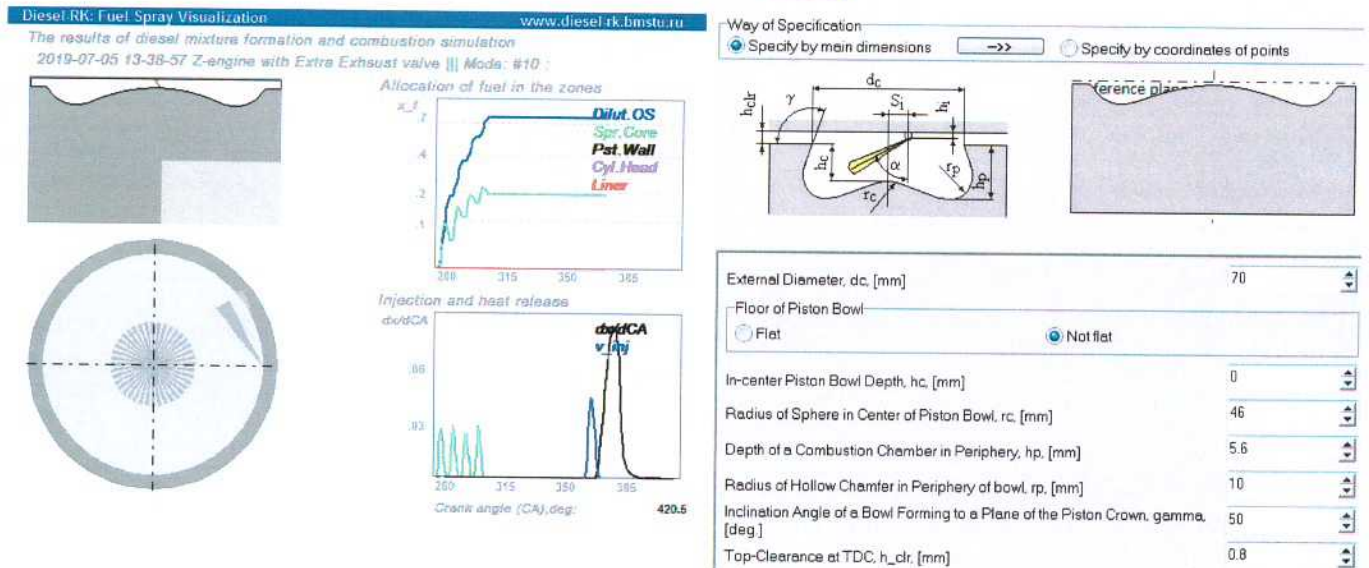
- Combustion chamber geometry is presented in fig.1.



Figure - 1. Combustion chamber for Z-engine*

*This piston bowl provides CR = 24. If necessary it is possible to make the bowl little bit more shallow in periphery to increase possible CR up to 26 or more.

Z-engine parameters at max torque mode are presented in Appendix 1.

Max Torque Power: 82.73 kW @ 1500 RPM;

BMEP = 32.58 bar;

p max= 235.7 bar;

T max= 1745.4 K;

Parameters of heat exchange in the cylinder:

T eq = 921 K;

Heat transfer coefficient:  htc = 693 W/m2/K.

## 2) Targets of the investigation:

- The first piston ring temperature has to be less than 200 C;

- The average piston head temperature at the fire surface should be about 427 K.

3) **Steps of investigation**

- Development of the piston 3D model on the base of pistons of similar existing engines;

- Analysis of temperature field of developed piston (0-iteration);

- Calibration of the FEA model for prototype's piston (to get boundary conditions in combustion chamber using Diesel-RK simulation and comparison with existing temperature field data);

- Simulation the "piston-cylinder liner" interaction to define the heat boundary conditions of piston skirt and rings;

- Analysis of temperature field on the maximum torque mode (1-iteration) and make some conclusions (modeling three different cooling modes: no cooling, spray jet cooling of the under skirt surface, jet cooling gallery)

- Creation of FE model for use in DIESEL-RK (with table to set BC of oil cooling for every operating mode) (not done);

- Investigation of the cooling gallery's geometry, numbers of the oil injectors, flow rate and etc;

- Modeling the temperature field on different engine's modes (not done).

- Estimation of stresses of the piston, with piston pin and connecting rod small end.

3) **The data being necessary for the investigation**

- In-cylinder parameters (T, p) for each mode;

- Combustion chamber heat boundary conditions for each mode.

Table №1

| mode | BMEP, bar | Peak pressure, bar | RPM | htc (Woschni), W/m$^2$K | $T_{eq\_cycle}$ (Woschni), K |
|------|-----------|--------------------|-----|-------------------------|------------------------------|
| 1    | 32.6      | 235                | 1500| 694                     | 921                          |
| ...  |           |                    |     |                         |                              |
| 10   |           |                    |     |                         |                              |

# I) Concept of steel piston from different manufactures

a) Federal-Mogul Monosteel pistons (fig. 2) [1].



Figure - 2. Monosteel piston from Federal-Mogul

Special characteristics:

- 250-bar and beyond firing pressure;
- friction-welded;
- a full-length skirt.

b ) KS Kolbenschmidt GmbH (fig. 3) [2]. Steelteks



Figure - 3. KS Kolbenschmidt Steelteks piston

–In contrast to friction-welded steel pistons, this piston is produced from a single forged part;

-KS Kolbenschmidt removes the need for welding beads in the cooling gallery, which disrupt and therefore reduce heat transfer [3].

-The material used is heat-treated steel 42CrMo4 [3].

- Due to machining limitations minimum groove heights for steel PC pistons are 2.0mm [4].

c ) Mahle's pistons [5]

FERROTHERM piston: The two parts, piston crown and piston skirt, are movably connected to each other through the piston pin. The piston crown, made of forged steel, the light aluminum skirt only bears the lateral forces. "Shaker cooling" via the skirt, closed cooling channels can also be incorporated in the piston crown. The outer cooling gallery of the steel piston crown is closed by split cover plates (fig. 4)



Figure - 4. Mahle FERROTHERM piston

MONOTHERM piston: This piston type is a single-piece forged steel piston that is greatly weight optimized as compared with FERROTHERM concept. The outer cooling gallery is closed off by two cover plate halves. The MONOTHERM® piston is used in commercial vehicle engines with peak cylinder pressures of up to 250 bar (fig. 5).



Figure - 5. Mahle MONOTHERM piston

MONOWELD piston: The structure is stiffer than the MONOTHERM piston, making for an increased thermal load capacity. The MonoWeld piston is suitable for peak cylinder pressures of up to 250 bar (fig. 6).



Figure - 6. Mahle MonoWeld piston

In a direct comparison between the MonoWeld and MONOTHERM concepts, a temperature reduction at the bowl rim by up to 70K could be achieved (fig. 7). This improvement is based on two aspects. One being the reduction of the wall thickness towards the bowl and the other aspect being the improvement of the hydraulic parameters in the cooling system of the piston by the closed cooling gallery [6].
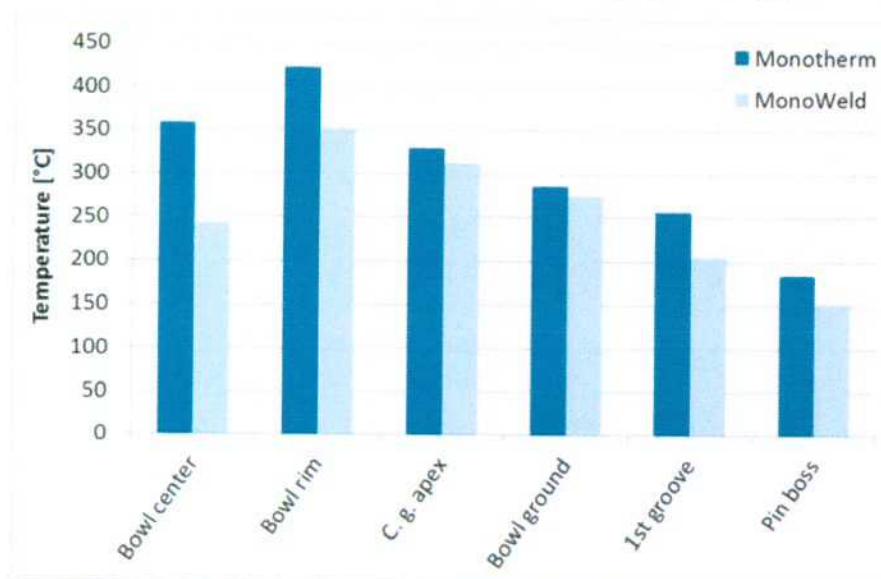


Figure - 7. Temperature measurement results Monotherm vs. MonoWeld at rated power and firing pressure 200 bar [6]

MONOLITE piston (fig. 8):

This concept based on a laser welding process. The MonoLite piston offers a high durability for P max beyond 230 bar. Key motivation of the piston development was a high degree of freedom for the design of the general compression height with regard to the load requirements and also to provide cooling gallery shapes and cross sections that give the best benefit in terms of bowl rim temperatures. Investigations have shown [6] that a reduced cross section as part of a cooling optimization can have positive effects on the cooling performance by increasing the catching efficiency and reducing the dwell time of oil in the gallery. Additionally, shapes such as a kidney like design or other geometries are possible to be manufactured with the laser welding process. E.g., smaller cross sections compared to a typical friction welded design and specific shapes that can be implemented, improve the overall cooling situation [6].



Figure - 8. Mahle MONOLITE piston

In back to back measurements of a friction welded and a laser welded piston, the results show a similar result in bowl rim temperatures even though the cooling gallery of the laser welded piston is about 38% smaller in this case (fig. 9). The weight of the laser welded version can be reduced by approximately 1.1 kg for a typical 130 mm diameter class piston.
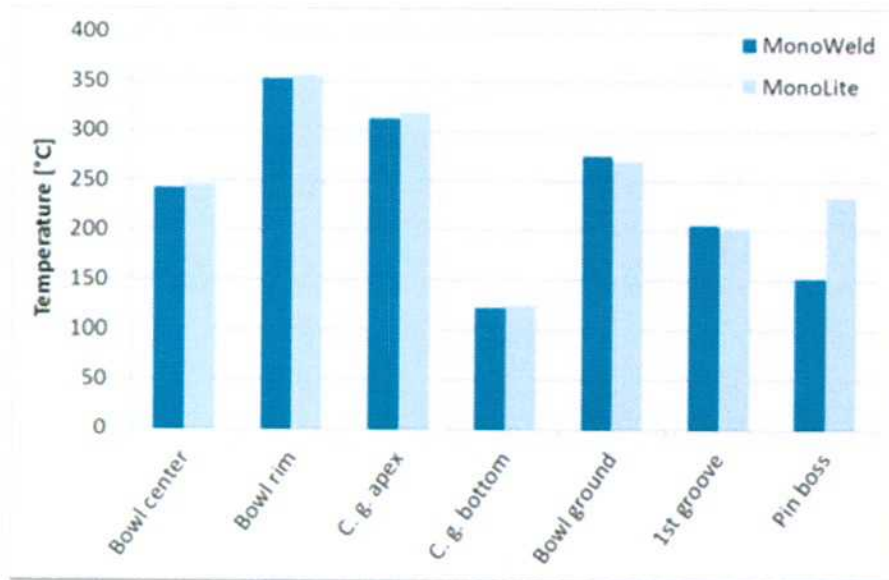
Figure - 9. Temperature measurement results MonoWeld vs. MonoLite [6]

The upper and lower part of the piston are joined at two positions, seam A and seam B. Seam A is located in the piston crown area and is pointing vertically to the cooling gallery zenith whereas the seam B is located in the lower bowl wall area pointing again towards the cooling gallery (fig. 10).
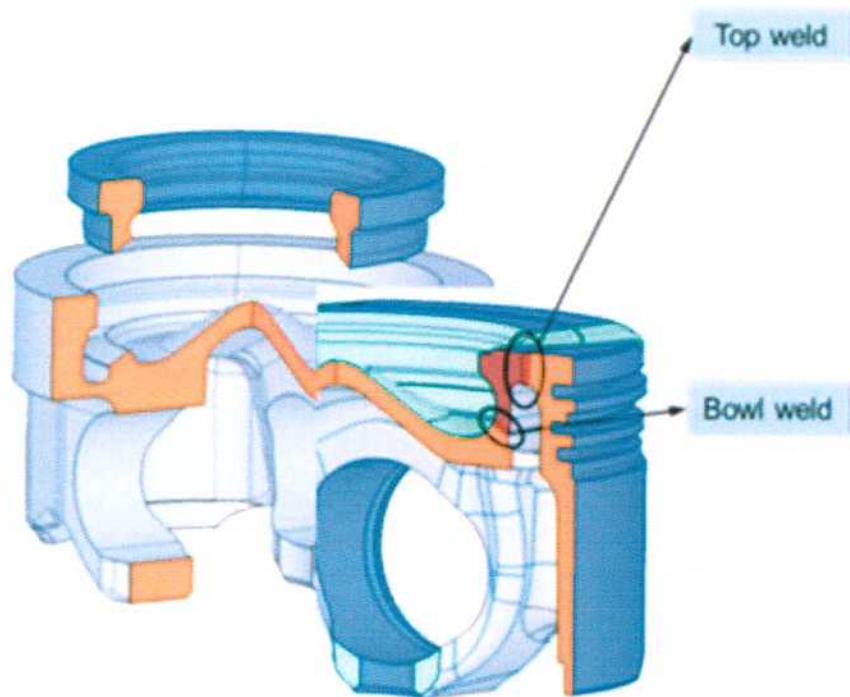


Figure - 10. Cut section of piston model with close up of weld seams

Engine trends and regulations such as EU VI and beyond are targeting for higher P max, which makes a full skirt piston a preferred solution. MAHLE developed for this purpose the MonoWeld friction welded piston, which offers not just a higher durability,

but as well an improved cooling efficiency [6]. The same conclusions were given in Federal-Mogul presentation (fig. 11).
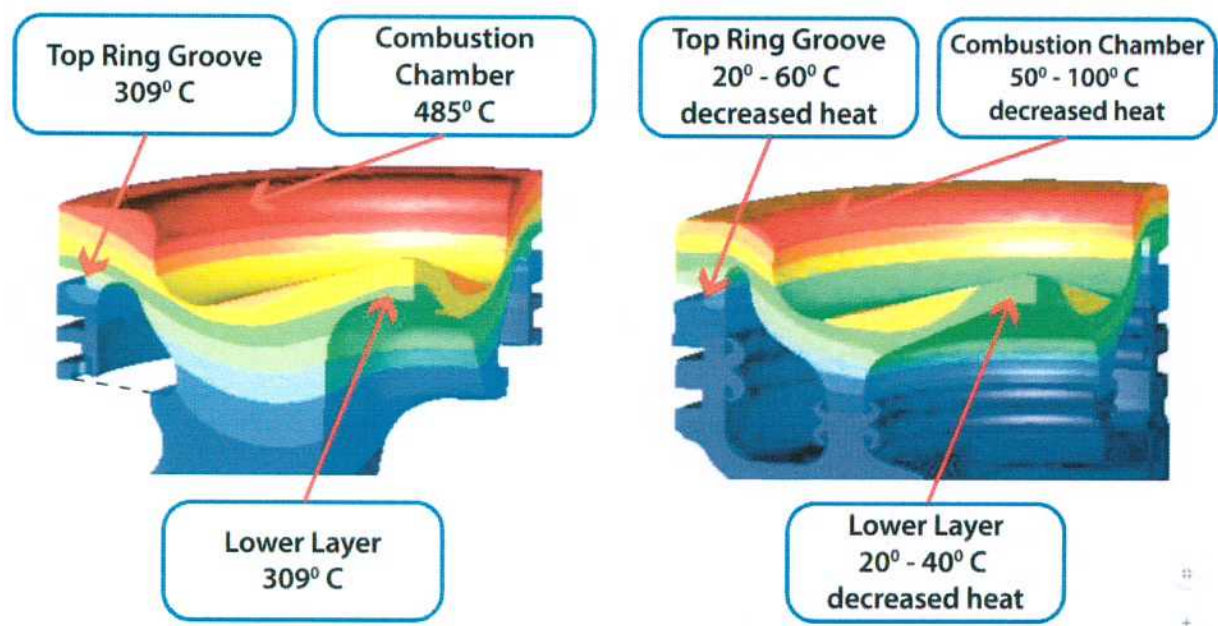


Top Ring Groove 309° C
Combustion Chamber 485° C
Lower Layer 309° C

Top Ring Groove 20° - 60° C decreased heat
Combustion Chamber 50° - 100° C decreased heat
Lower Layer 20° - 40° C decreased heat

Figure - 11. Federal-Mogul corporation's data [1]

A drawback of the friction welded piston is the necessary space to accommodate the weld seams and flesh with the according heat affected zone. From this point of view the laser welded solution of Mahle and KS Kolbenschmidt forged piston look preferable.

By my opinion we should consider single piece steel pistons with stiff structure like MonoWeld(Mahle), MonoLite(Mahle), Steelteks(Kolbenschmidt) and Mogul's Monosteel piston. On this step of investigation there are not a big different in such piston design in terms of temperature field (fig. 9). We will choose prototype engine no matter with forged laser-wet or friction-welded piston and if it's necessary we will change specific dimensions latter.

## II ) The 3D model of piston based on the piston of similar existing engine

- Prototype engine - Mercedes-Benz OM626 [3-4].

Engine characteristics:

Bore/stroke        82/92.3;

BMEP               25.8 bar;

P max              205 bar.

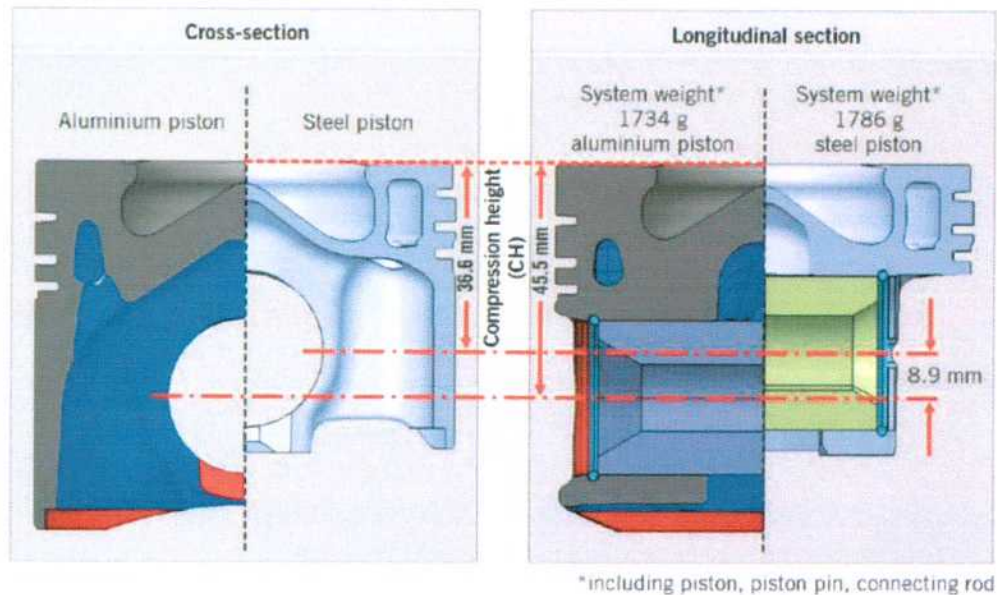Mercedes-Benz aluminum and forged steel pistons (fig. 12)



Figure - 12. Mercedes-Benz OM626 pistons*

**\* The aluminum piston on the left side and the steel piston on the right side**

The geometry of pistons was restored and redesign for our object of investigation (fig. 13).
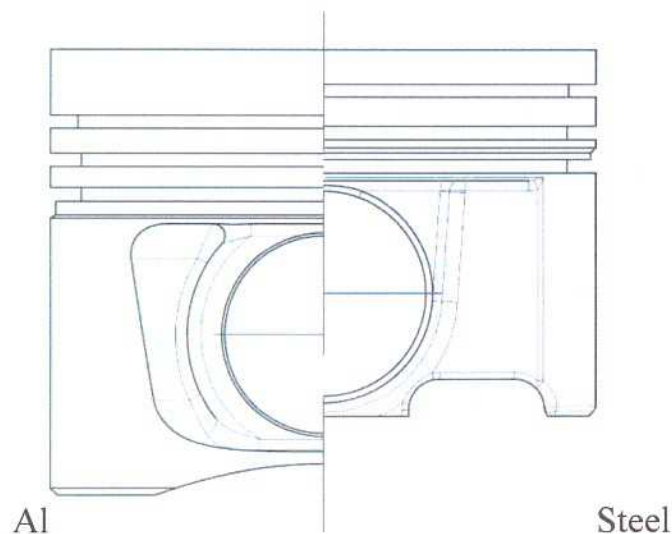


Figure - 13. Mercedes-Benz OM626 pistons (models from pictures)

There is no data in literature about steel piston characteristics dimensions but we can compare Al-piston dimensions Mahle's recommended values [5, 7] and after that reconstruct steel piston by fig. 12 in the true scale.

Some dimensions have been improved for CR = 24 and shallow combustion chamber. The full geometry model of piston was present on following picture (fig. 14).
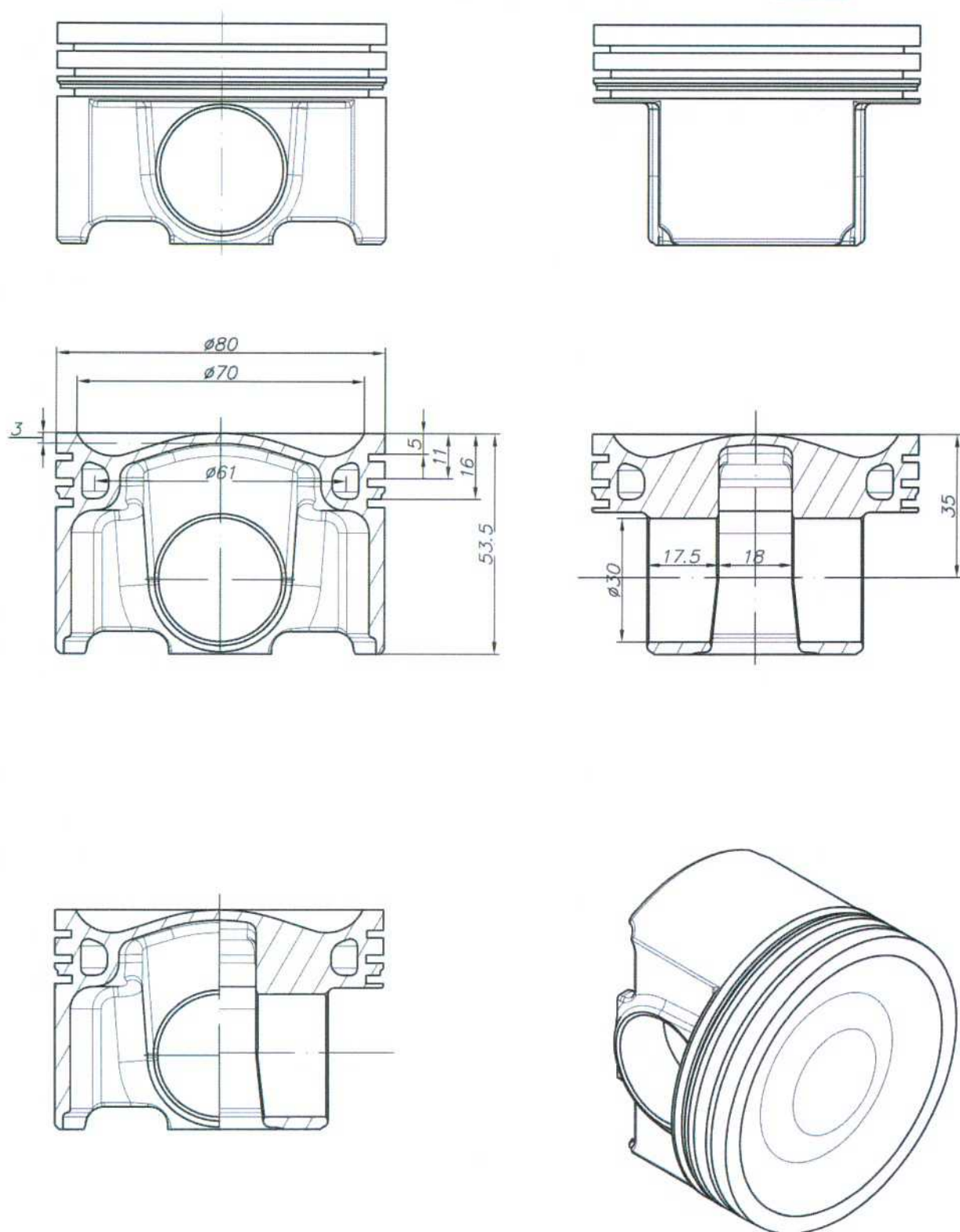


Figure - 14. Sketches of the forged steel piston for Z-engine

### III ) Analysis of the piston's temperature field at max torque mode
### - Model for prediction a gallery oil filled ratio and necessary oil flow

The cooling gallery model was developed based on the prediction of the oil fill ratio (OFR), which represents how much the cooling gallery is filled with coolant. The model assumes a one-dimensional orifice with infinite length and the OFR is given as [8]. The filling ratio OFR is a dimension for the expected cooling effects due to the shaker effect in a partially filled cooling channel (fig. 15) and is defined as:

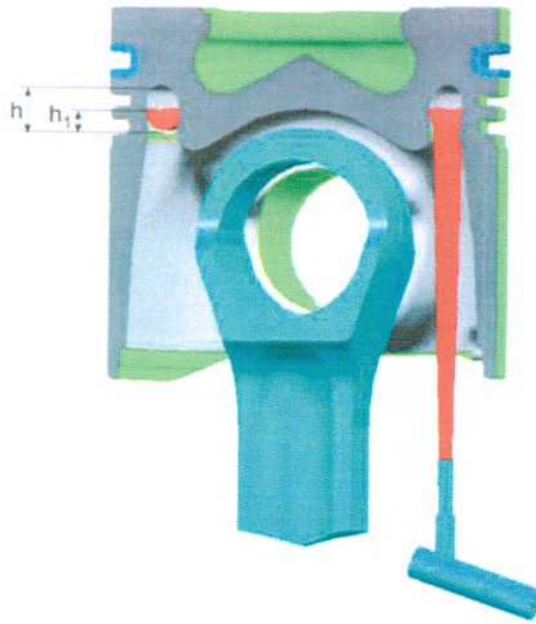$$OFR = \frac{V_1}{V} \approx \frac{h_1}{h} \tag{1}$$



Figure - 15. Definition of the filling ratio

An intensive convective heat transmission arises in the cooling gallery of the moving piston due to the shaker effect, which can be attributed to the highly turbulent mixing motion that enhances energy exchange. A completely filled cooling channel or cooling gallery would exhibit a lower heat transmission coefficient as a result of the lower oil velocities. Basic tests with a heated model show that the filling ratio affects the heat transmission coefficient (fig. 16).

The optimal filling ratio is 30 to 60%. In this case, the heat transmission coefficient drops off again above a filling ratio of 60%, due to the reduced turbulence in the channel filled to a higher level.

$$\dot{q} = \alpha(T_W - T_{oil})$$

$\dot{q}$ = Specific heat flux

$\alpha$ = Heat transfer coefficient

$T_W$ = Wall temperature

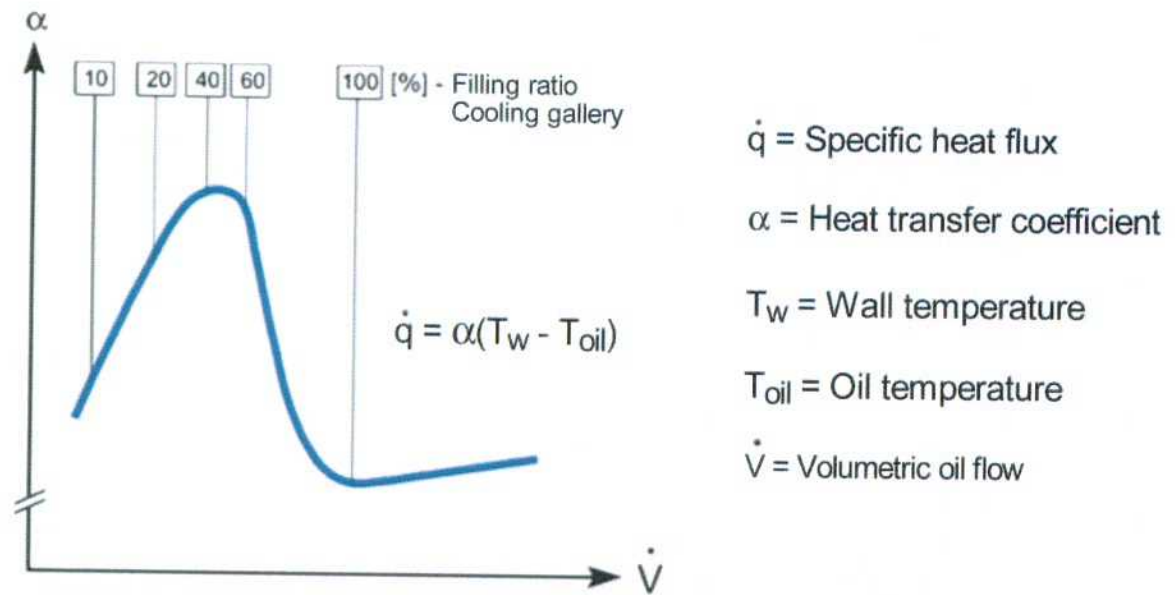$T_{oil}$ = Oil temperature

$\dot{V}$ = Volumetric oil flow

Figure - 16. Relationship of filling ratio and heat transmission [5]

The mass conservation law for oil in gallery describes as (fig. 17):

$$S_g \cdot dh_1 = (Q_{inlet} - Q_{out})dt, \tag{2}$$

here $Q_{inlet}$, $Q_{out}$ the flow rates of coolant coming in and going out of the cooling gallery, respectively and $S_g$ is the area of the horizontal sections of the cooling gallery.
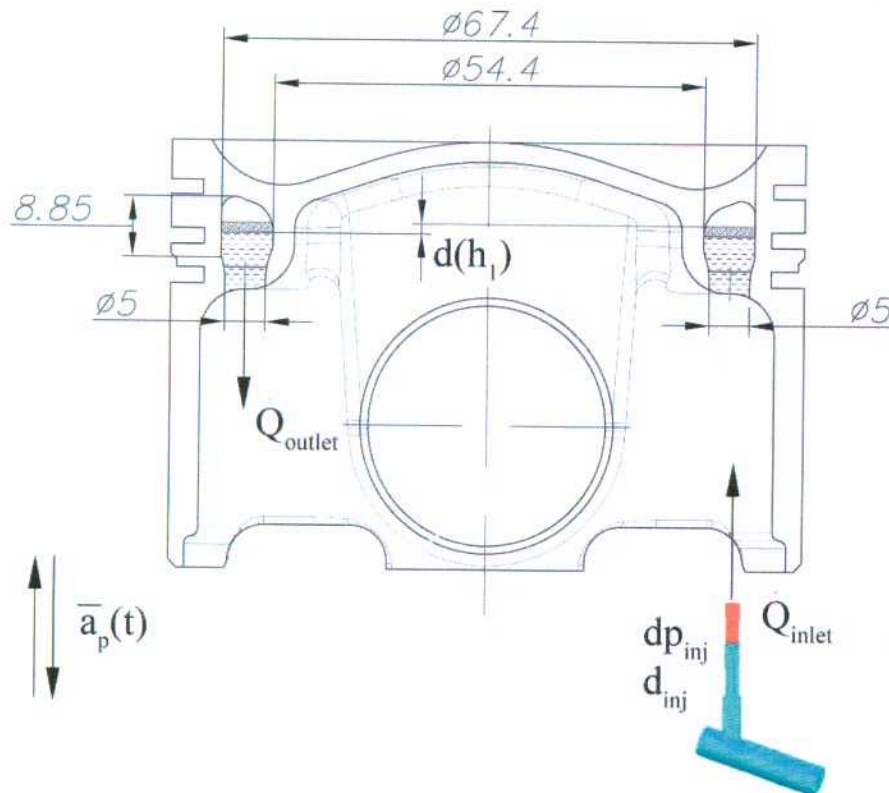


Figure - 17. Computational model for prediction a gallery oil filled ratio

The flow rates of supply oil can be calculated as follows with outlet area of oil jet, oil pressure, oil density and flow loss coefficient($\mu_f$):

$$Q_{inlet} = \mu_f \cdot \frac{\pi \cdot d_{inj}^2}{4} \cdot \sqrt{\frac{2 \cdot dp_{inj}}{\rho_{oil}}} ; \tag{3}$$

The outlet flow from cooling gallery $Q_{out}$, given by:

$$Q_{out} = \mu_{f\_out} \cdot \frac{\pi \cdot d_{out}^2}{4} \cdot V_{out} = \mu_{f\_out} \cdot \frac{\pi \cdot d_{out}^2}{4} \cdot \sqrt{2 \cdot a_p \cdot h_1} , \tag{4}$$

here $a_p$ - acceleration of piston (fig. 18).

$$a_p = -\varpi^2 \cdot \frac{S}{2}(\cos(\varphi) + \lambda \cos(2\varphi)), \tag{5}$$

here $\varpi$ - engine angular velocity, $S$ - engine stroke, $\varphi$ - crank angle.
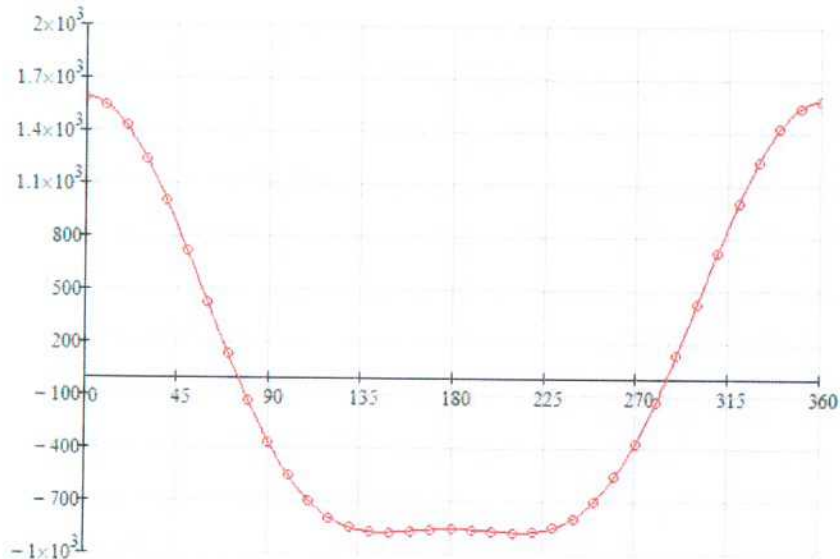


Figure - 18. Acceleration of the Z-engine's piston

If we will take into account recommendations from [5] we should have filling ratio is about 60%. Let's guess that the oil supply pressure is 3 bar for our case. The oil supply velocity is:

$$V_{inlet} = \sqrt{\frac{2 \cdot dp_{inj}}{\rho_{oil}}} = 25.0 \text{ m/s}$$

The expression (2) is ordinary differential equation (ODE) with the unknown oil level in gallery - $h_1$. This equation can be solved by simple Euler forward method. Using the

filling ratio is equal to 60% as the target, we will get the oil volumetric flow rate $Q_{inlet}$ = 2.2 L/min per cylinder and the injector diameter $d_{inj}$=1.5mm (fig. 19).
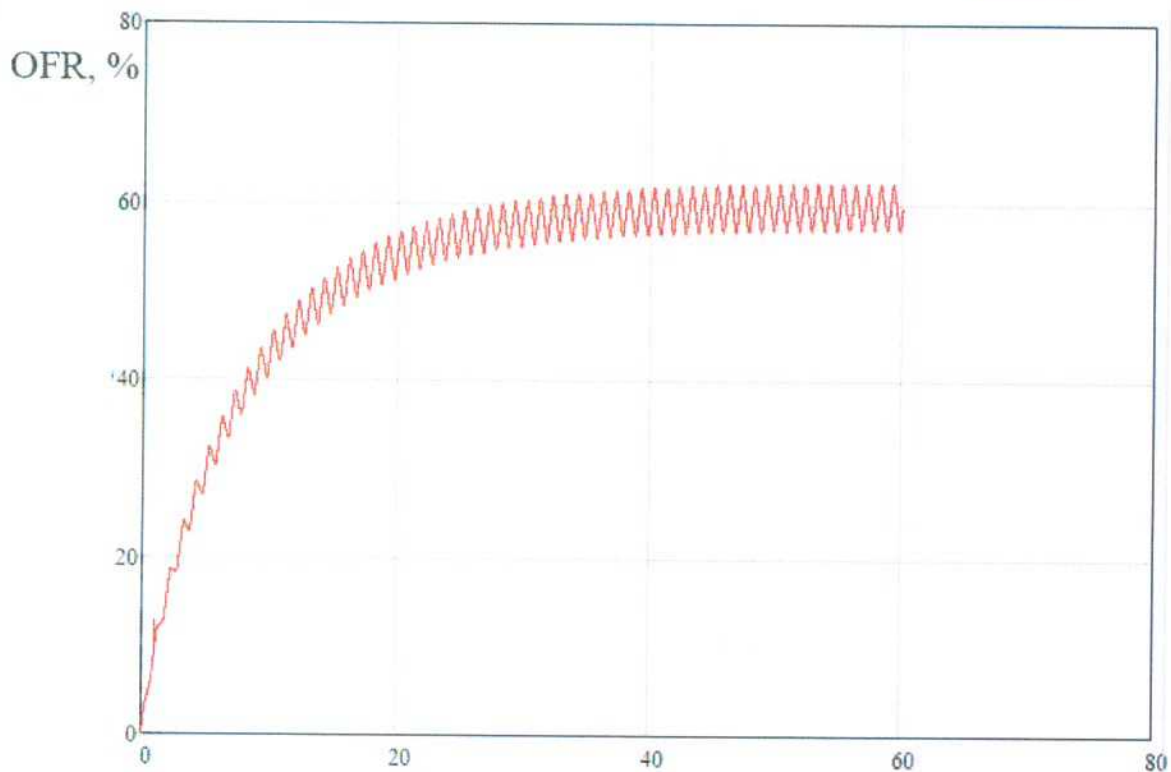


Figure - 19. The oil fill ratio in respect of number of crankshaft revolution

If we need we can check desirable oil volumetric flow rate by CFD calculations later.

- Testing of the CFD prediction model of filling the gallery and the heat transfer coefficient

The main idea of this simulation is to check possible of using CFD code for determine the coefficient of heat transfer in gallery at full task. It means that we are modeling piston motion, jet penetration in under the piston space and the filling of piston gallery.

The FE model is present on figure 20 and consists from about 3 million polyhedral cells. Piston motion is modeled by layering technique which allows to add or remove layers of cells adjacent to a moving boundary, based on the height of the layer adjacent to the moving surface.

Oil supply conditions were choice overestimated. The oil supply velocity is 30 m/s, and the injector diameter is 2.5 mm. I just wanted to check the model and tried to fill gallery in two strokes.

Oil jet reached gallery wall at 18 degree and outlet hole on the opposite side of piston at 230 degree (fig. 21). The full video of oil propagation is attached to the letter.



a                                                                    b
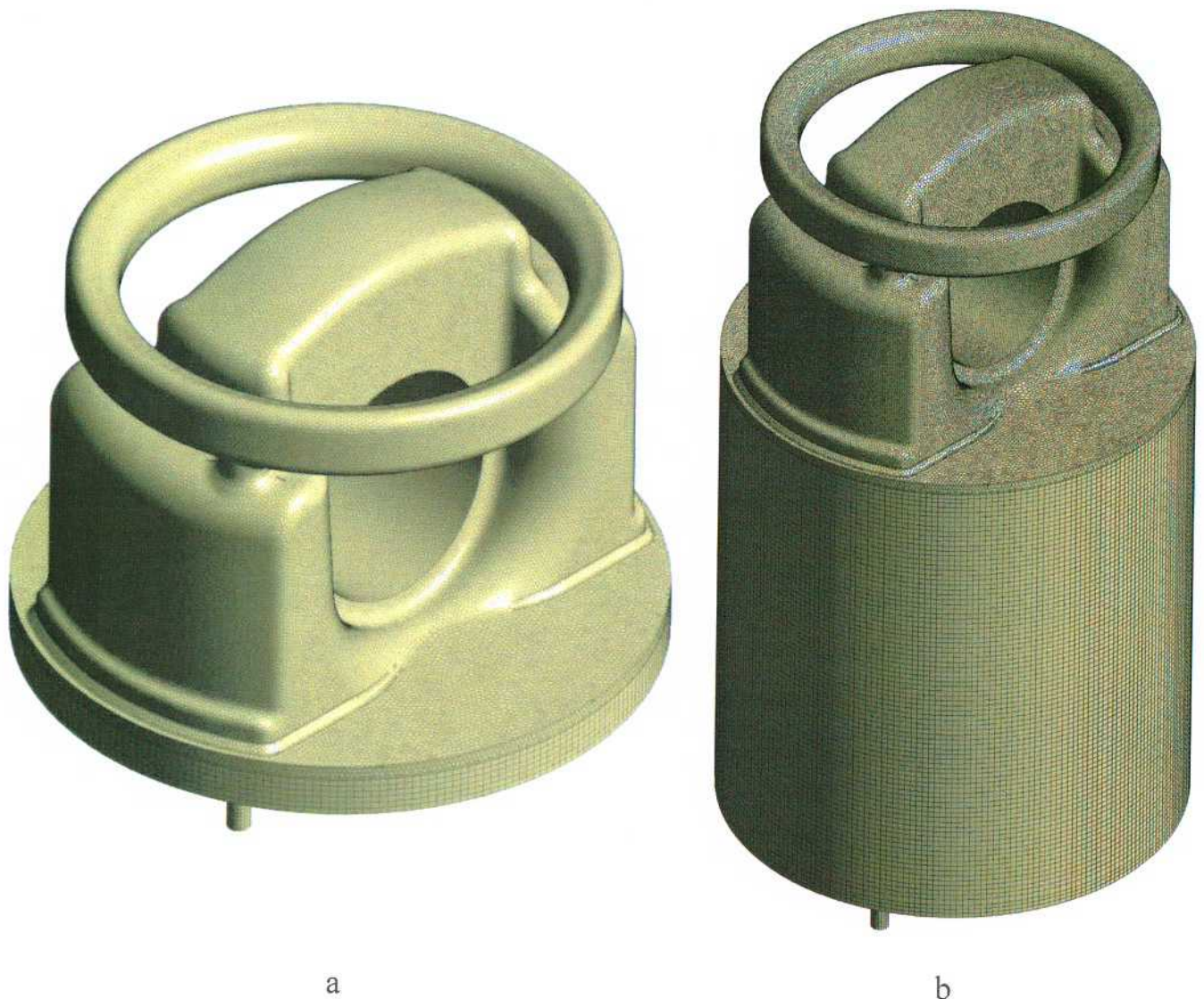
Figure - 20. FE model of under the piston space:

a) -at BDC position, b) - at TDC position

Solution time is 2.5-3 days for two stroke motion. As you can see from figure 19 the time for filling gallery is about 30-40 strokes. In this situation I recommend to investigate influence of the OFR on the heat transfer coefficient using 2D simulation of gallery with different level of OFR and after that extrapolating result on 3D thermal model of piston.

We may use 3D simulation of oil motion in next few cases:

- to verify the oil supply flow rate and the empirical model for prediction gallery oil filled ratio;

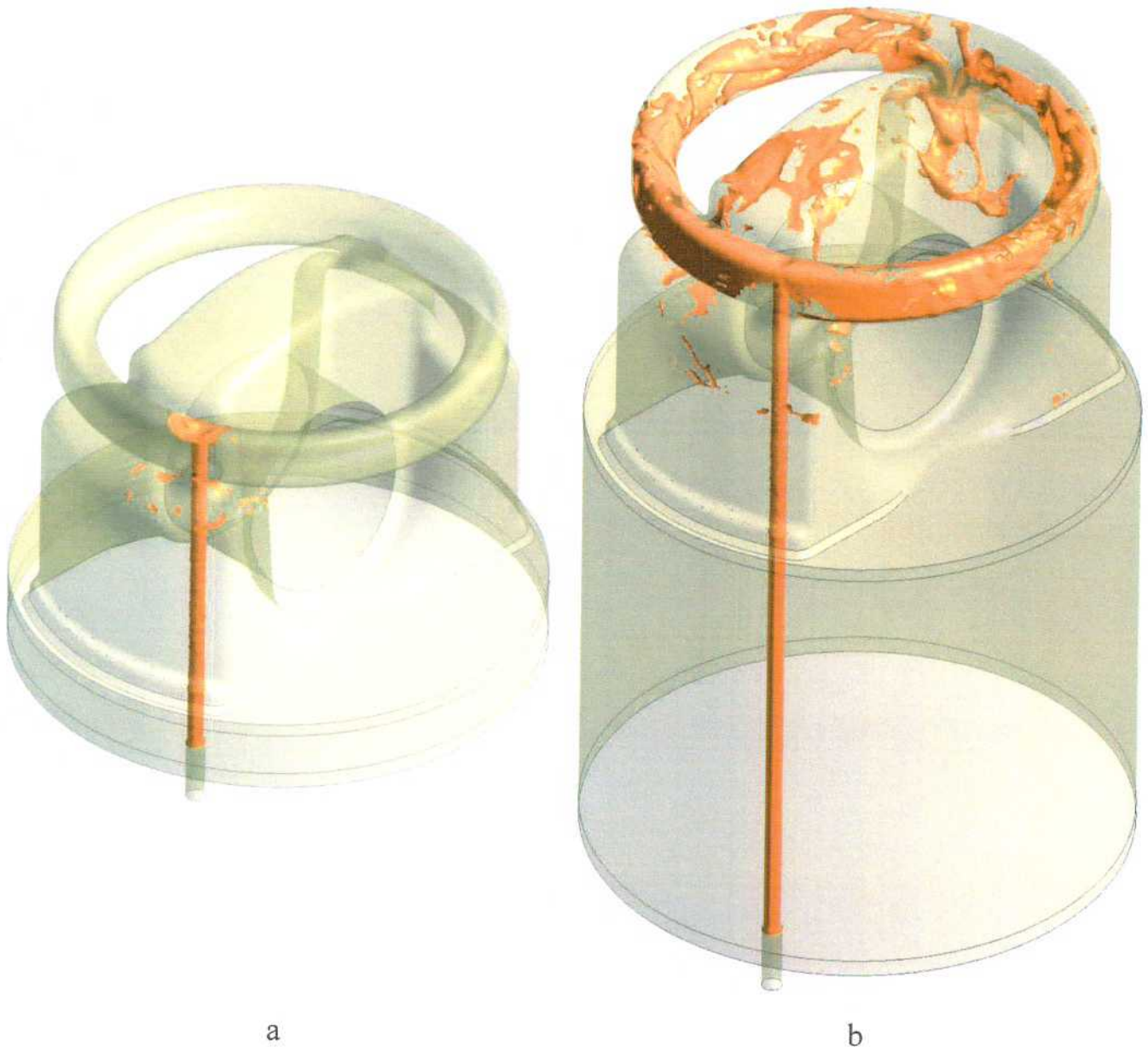- to make final calculation of piston temperature filed for checking results.

a                                                                    b

Figure - 21. Oil jet penetration:

a) -reached gallery, b) - reached gallery outlet hole

## - The analysis of temperature field (0-iteration)

First of all we need to prepare FE model based on existing 3D model of piston. ANSYS Inc software will use for all simulations. The FE model consists from about 10 thousand free hex-dominated mesh elements (fig. 22).

Boundary conditions (BCs) for thermal task should be divided by zone with different dominant mechanism of heat transfer.

- The piston ring set zone and the associated ring land surfaces on the cylinder wall;

- The inner contour of the piston;

- The cooling gallery zone;
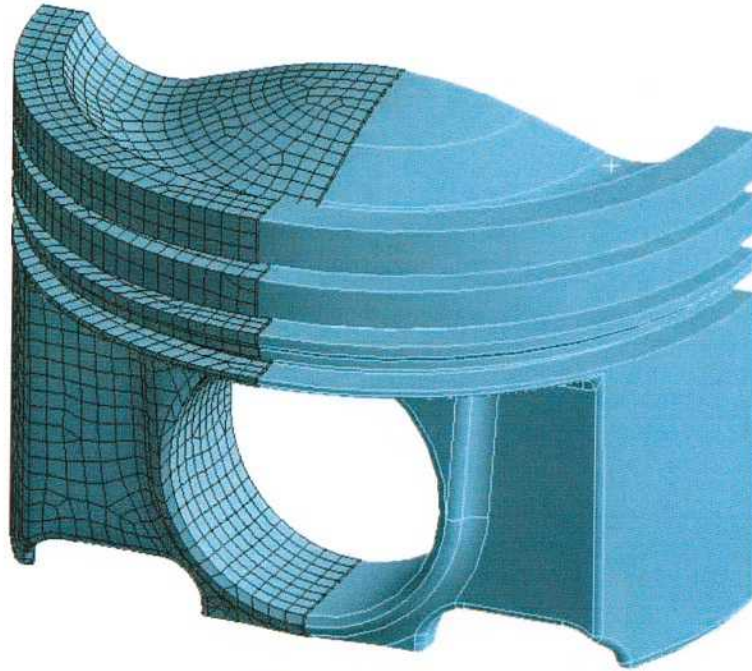- The piston skirt zone;
- Combustion chamber zone.



Figure - 22. FE model of the piston

**Combustion chamber zone**

Here, the average heat transfer coefficient (htc) and equivalent temperature are determined using Woschni correlation. For Z-engine at max torque mode is equal to:

T eq = 921 K;

$htc_{av}$ = 693 W/m2/K.

Although Z-engine realizes HCCI-combustion process it has 10 % pilot doze of diesel fuel. It means that we should consider boundary condition not for full homogenical case but using distribution like for diesel process by 10 %. An empirical data available from [9] can be applied to derive the htc along the radial direction of the fire surface of a diesel piston (fig. 23).

After distribution procedure we need to check heat flux balance for all discrete zones in form of:

$$htc_{av} \cdot T_{eq} \cdot S_{piston} = \sum_{i=1}^{N} htc_i \cdot T_{eq} \cdot S_i ,$$ (6)

here $htc_i$ and $S_i$ - heat transfer coefficient and area of the i-zone, respectively.

We have the following distribution for Z-engine (Table №2):

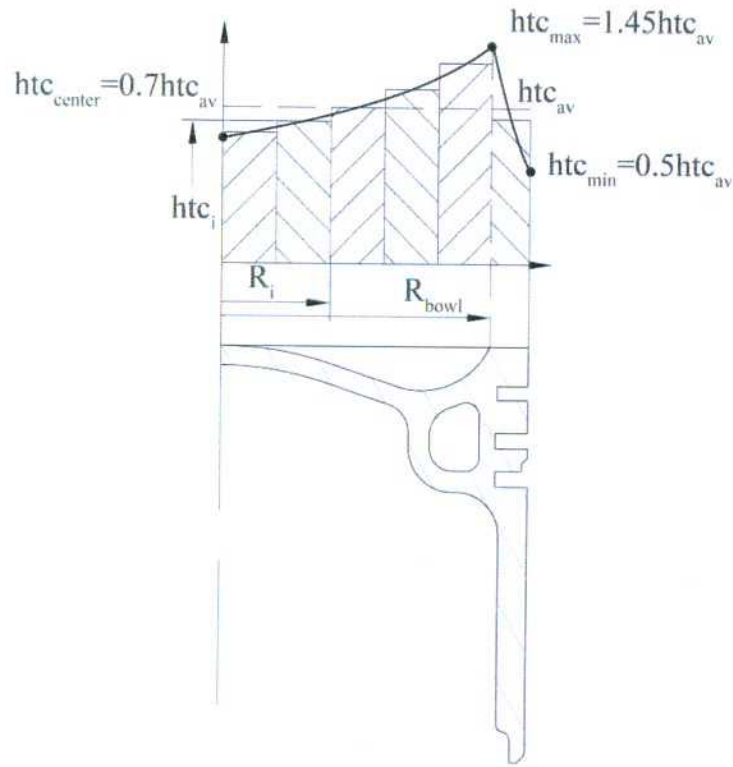$$htc_i^{Z-engine} = 0.1 \cdot htc_i^{diesel} + 0.9 \cdot htc_{av} \qquad (7)$$



Figure - 23. Heat transfer coefficient distribution along the radial direction of a diesel piston

Table №2

| Zone | R1, mm | R2, mm | htc, W/m2/K | T, K |
|------|--------|--------|-------------|------|
| 1 | 0 | 7 | 679 | 921 |
| 2 | 7 | 14 | 681 | 921 |
| 3 | 14 | 21 | 686 | 921 |
| 4 | 21 | 28 | 695 | 921 |
| 5 | 28 | 35 | 707 | 921 |
| 6 | 35 | 40 | 686 | 921 |

**Oil gallery cooling zone**

In paper [10] model for prediction heat transfer coefficient in the cooling gallery have been developed. In the model, coolant in the cooling gallery goes through three phases, acceleration, impaction, and bouncing=dissipation, during the piston's travel from top dead center (TDC) to bottom dead center (BDC) (fig. 24).
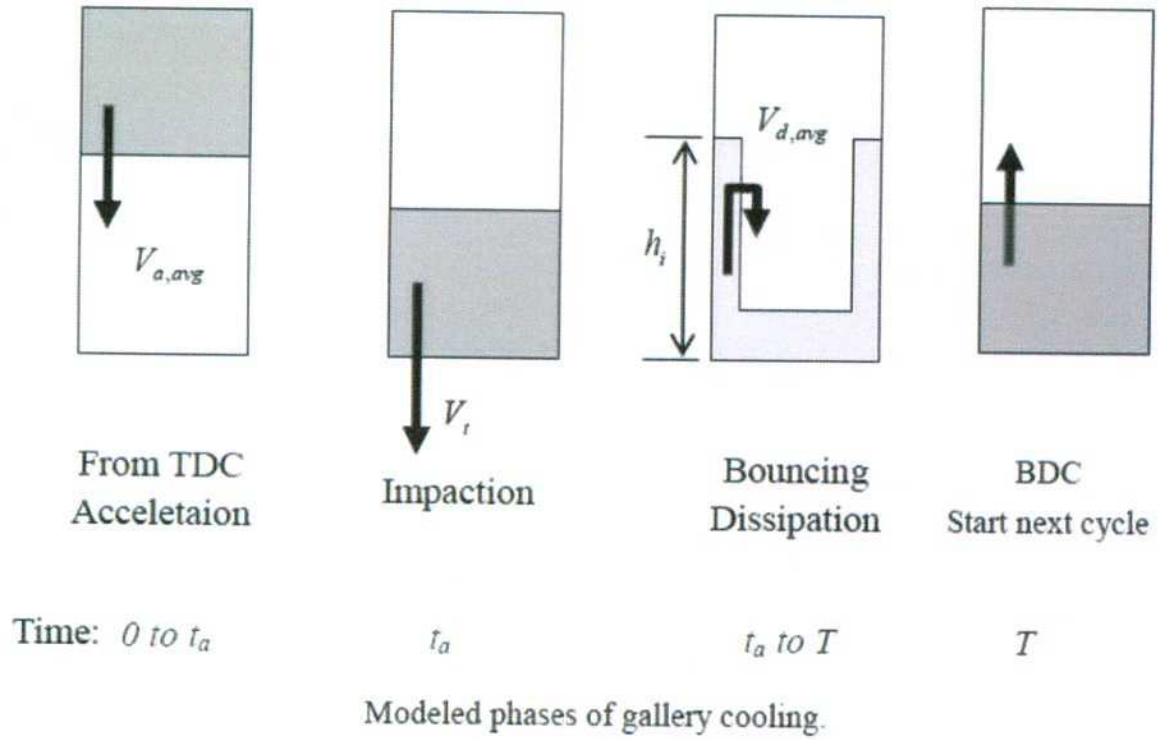
Modeled phases of gallery cooling.

Figure - 24. Cooling gallery model with OFR and cocktail shaker effects [10]

The start of the cooling phase is set at TDC. The bulk of the coolant's increase in velocity is due to the piston's acceleration from TDC to BDC (fig. 18) until it reaches the opposite horizontal wall in the gallery, and the time of duration in the acceleration phase is denoted as $t_a$:

$$t_a = \sqrt{\frac{2 \cdot h_c \cdot (1 - OFR)}{a_{p.av}}} \tag{8}$$

here $h_c$ - the height of the cooling gallery, $a_{p.av} = \frac{S}{2} \cdot \frac{\omega^2}{\pi}$ - is the average acceleration during the acceleration phase.

The average velocity of coolant during the acceleration phase:

$$V_{a.av} = \frac{h_c \cdot (1 - OFR)}{t_a} \tag{9}$$

The terminal velocity of the coolant hitting the wall, are estimated to be:

$$V_t = a_{p.av} \cdot t_a \tag{10}$$

During the acceleration phase, it can be assumed that the cooling effect is due to plug flow in the closed channel [10]. Therefore, the Nusselt number $Nu_a$, and the heat transfer coefficient, $HTC_a$, are obtained by [11]:

$$Nu_a = \begin{cases} 3.65 \dfrac{0.104 \cdot \dfrac{D_h}{h_c} \cdot \text{Re}_a \cdot \text{Pr}_{oil}}{1 + 0.016(\dfrac{D_h}{h_c} \text{Re}_a \cdot \text{Pr}_{oil})^{0.8}} & if \quad \text{Re}_a = \dfrac{V_{a.av} \cdot D_h}{\upsilon_{oil}} \leq 2000 \\[6mm] 0.023 \cdot \text{Re}_a^{4/5} \cdot \text{Pr}_{oil}^{0.3} & if \quad \text{Re}_a > 2000 \end{cases} \qquad (11)$$

and

$$HTC_a = k_{oil} \frac{Nu_a}{D_h} \qquad (12)$$

where $\text{Pr}_{oil}=257.7$ is the Prandtl number, $\upsilon_{oil}=1.93e\text{-}05$ is the kinematic viscosity, and $k_{oil}=0.132$ is the thermal conductivity of the coolant oil (SAE-30). $D_h = 2(R_2 - R_1)$ is the horizontal hydraulic diameter (for our case $R_2 = 67.4/2$ and $R_1 = 54.4/2$ - figure 17). $\text{Re}_a$ is the Reynolds number during the down-stroke of the piston.

During the impaction stage, the coolant hits the wall at velocity $V_t$ and the energy imparted by the piston is dissipated by the fluid bouncing back to the other side. From the time of the end of the acceleration (which is at the time of start of impaction), to BDC, the average coolant velocity is obtained by a momentum balance as [10]:

$$m \frac{dV}{dt} = -\mu_{oil} \cdot V \qquad (13)$$

here $m = \rho_{oil} \cdot h_c \cdot \pi(R_2^2 - R_1^2)$ - is the total mass of coolant in gallery.

Thus, the $V_{i.av}$ is average velocity of the oil during the time from start of impaction to BDC ($t_i = T_{cycle} - t_a$):

$$V_{i.av} = \frac{V_t}{t_i} \frac{m}{\mu_{oil}} \left(1 - \exp(-\frac{\mu_{oil}}{m} t_i)\right) \qquad (14)$$

The same result (14) can be obtained by numerical solving of ODE (13). The Nusselt number $Nu_i$, and heat transfer coefficient $HTC_i$, during the impaction and bouncing phases are estimated to be [11]:

$$\text{Re}_i = \frac{V_{i.av} \cdot D_h}{\upsilon_{oil}} \qquad (15)$$

$$Nu_i = 0.69 \cdot \text{Re}_i^{0.5} \cdot \text{Pr}_{oil}^{0.4} \qquad (16)$$

$$HTC_i = k_{oil} \frac{Nu_i}{D_h} \qquad (17)$$

The effective height that the coolant can bounce up in the gallery $h_b$ could be obtained from mechanical energy balance:

$$\frac{1}{2} m \cdot V_{i.av}^2 = m \cdot a_{p.av} \cdot h_b \qquad (18)$$

The circumferential velocity of the coolant accounting for the OFR effect $V_c$:

$$V_c = \frac{1}{2} Q_{inlet} \cdot \frac{4}{OFR \cdot \pi \cdot D_{eqv}^2} \qquad (19)$$

here $D_{eqv}$ - is the hydraulic diameter of the gallery in the circumferential direction.

The Nusselt number of the circumferential flow $Nu_c$, and the heat transfer coefficient, $HTC_c$, are calculated as [11]:

$$Nu_c = \begin{vmatrix} 3.65 \dfrac{0.104 \cdot \dfrac{2D_{eqv}}{\pi(R_2 + R_1)} \cdot \mathrm{Re}_c \cdot \mathrm{Pr}_{oil}}{1 + 0.016(\dfrac{2D_{eqv}}{\pi(R_2 + R_1)} \mathrm{Re}_c \cdot \mathrm{Pr}_{oil})^{0.8}} & if \quad \mathrm{Re}_c = \dfrac{V_c \cdot D_{eqv}}{\upsilon_{oil}} \le 2000 \\[4ex] 0.023 \cdot \mathrm{Re}_c^{4/5} \cdot \mathrm{Pr}_{oil}^{0.3} & if \quad \mathrm{Re}_c > 2000 \end{vmatrix} \qquad (20)$$

and

$$HTC_c = k_{oil} \frac{Nu_c}{D_{eqv}} \qquad (21)$$

Considering the exposure time, the void area represented by OFR, and the applicable heat transfer coefficients, the average heat transfer coefficient in the cooling gallery, $HTC_{eff}$, is given as:

$$HTC_{eff} = \frac{HTC_a \cdot OFR \cdot (A_1 + A_2) \cdot t_a}{(A_1 + A_2 + 2 \cdot A_h) \cdot T_{cycle}} + \frac{HTC_c((A_1 + A_2)OFR + A_h) \cdot T_{cycle}}{(A_1 + A_2 + 2 \cdot A_h) \cdot T_{cycle}}$$
$$+ \frac{HTC_i \cdot t_i \left( A_h + \dfrac{h_b}{h_c}(A_1 + A_2) \right)}{(A_1 + A_2 + 2 \cdot A_h) \cdot T_{cycle}} + \frac{HTC_{air}((A_1 + A_2) \cdot (1 - OFR) + A_h) \cdot T_{cycle}}{(A_1 + A_2 + 2 \cdot A_h) \cdot T_{cycle}} \qquad (22)$$

here $A_h = \pi(R_2^2 - R_1^2)$ - area of the horizontal gallery surface, $A_1 = 2\pi R_1 \cdot h_c$ - the area of the inner gallery, $A_2 = 2\pi R_2 \cdot h_c$ - the area of outer surface of the gallery.

The first term of equation 22 is due to the acceleration motion of oil, the second term is due to circumferential motion of oil, the third term presents during impact phase and the fourth is a free convection to air in the gallery ($HTC_{air}$=150 W/m²/K).

The measurement results shown [8] a decrease in the heat transfer coefficient around the region with less amount of oil. The trend in the prediction does not correspond well with the measurement. In the region of small amount of oil, the raising of the cooling oil temperature is significant and the falling of the heat transfer coefficient becomes apparent.

We will take it into account by predicting of change oil temperature. Let's assumed that the average surface temperature of piston gallery $T_{p.av}$ can be obtained by iteration analysis of piston temperature field using $HTC_{eff}$ at the first step. Changing in oil temperature is described by heat conservation law:

$$HTC_{eff}\left(T_{p.av} - T_{oil}\right) \cdot S_{cont} \cdot dt = \frac{1}{2} C_{p.oil} \cdot Q_{inlet} \cdot \rho_{oil} \cdot dT_{oil} \qquad (23)$$

This ODE can be solved using by Euler forward method (fig. 25).



$T_{oil}$

Time of the oil travel
from the enter of gallery to exit
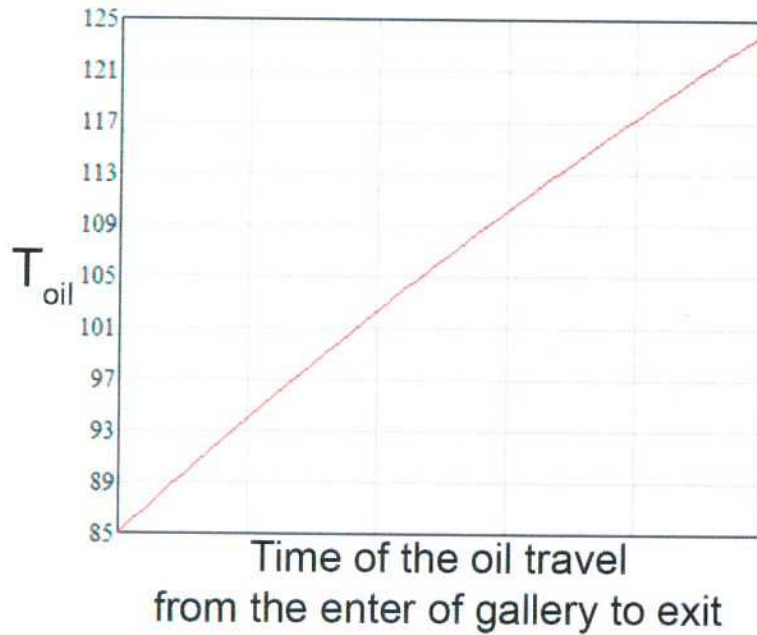
Figure - 25. Changing in oil temperature (OFR=0.050)

The HTC should be corrected by following expression:

$$HTC_{eff\_t} = HTC_{eff} \cdot \frac{\left(T_{p.av} - T_{oil.inlet}\right)}{\left(T_{p.av} - T_{oil.av}\right)} \qquad (24)$$

here $T_{oil.inlet}$ - oil temperature on inlet ($85^0C$), $T_{oil.av}$ - average oil temperature in gallery.

Resulted dependencies of heat transfer coefficient upon flow rate and OFR is showed on figure 26.
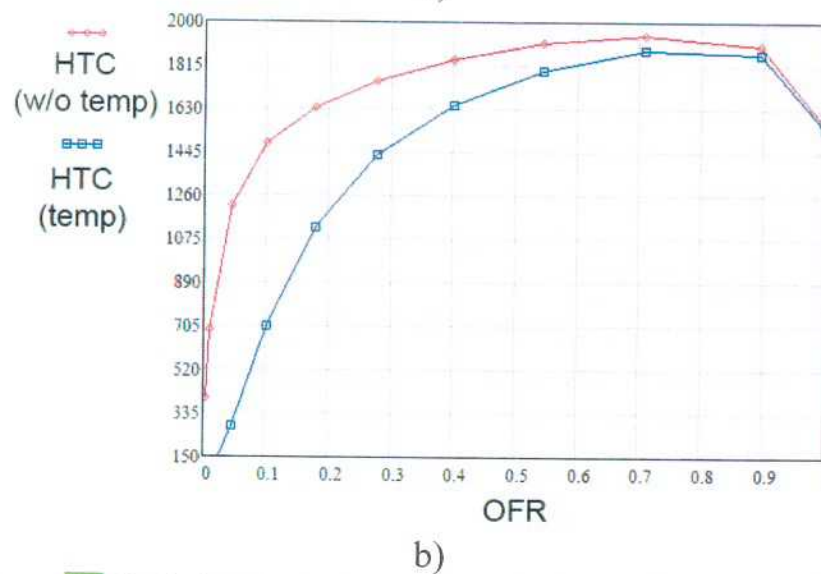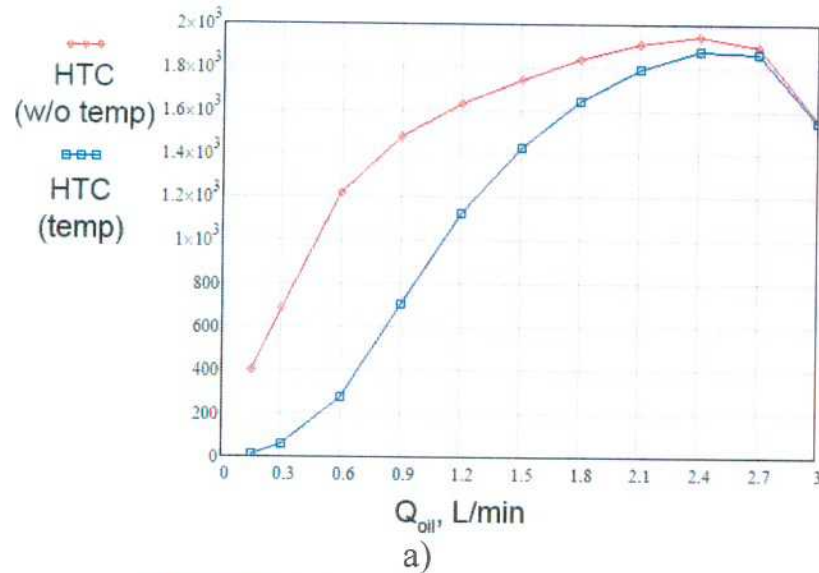
Figure - 26. Relationship between coefficient of heat transfer and:

a) cooling oil flow b) OFR

For chosen level of OFR (0.6) the heat transfer coefficient to oil ($HTC.g$) is equal to 1832 W/m²/K.

### The inner contour of the piston

The coefficient of heat transfer between the air ($T_{air}=85^0$C) below the piston and the piston surface, $HTC_{air}$ is 150 W/m²/K.

### The piston skirt zone

For initial approximation we will use the simple equation to determinate $HTC_{sk}$ by typical of cylinder gap height $\delta_{cyl}$ (about 0.050mm fig. 27[4, 14]):

$$HTC_{sk} = \frac{k_{oil}}{\delta_{cyl}} \approx 3000 \ \text{W/m}^2\text{/K} \qquad\qquad (25)$$



a)                        b)
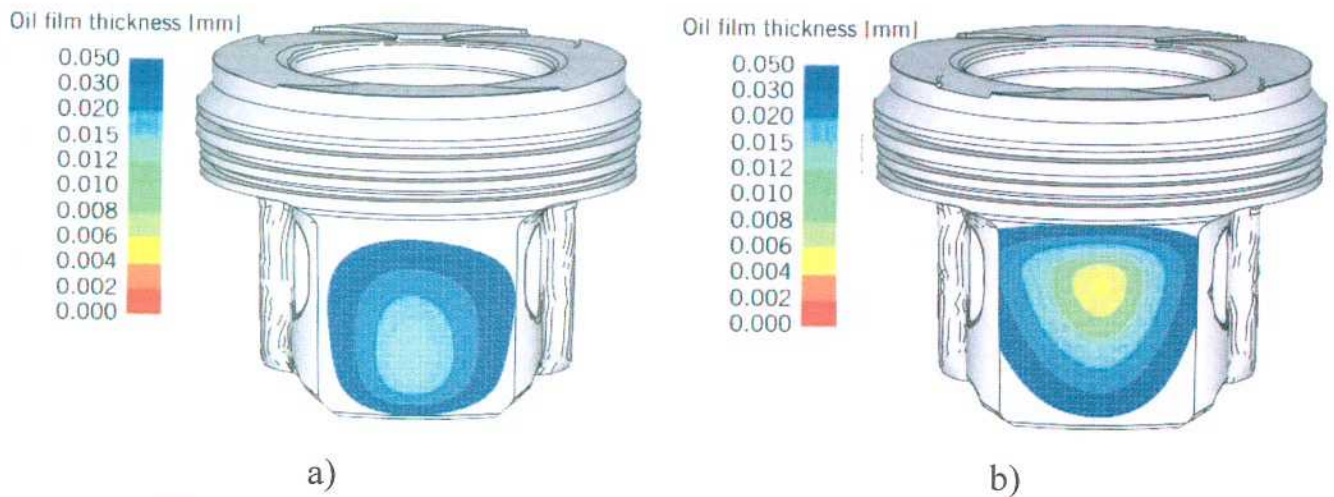
Figure - 27. Oil fi lm distribution at piston skirt and frictional mean effective pressure FMEP for aluminium and steel pistons at 1500 rpm, IMEP = 400 kPa [4]:

a) - Thrust side; b) - Antithrust side

**The piston ring set zone and the associated ring land surfaces on the cylinder wall**

For initial approximation we will use recommendations [12] to determinate heat transfer boundary conditions (fig. 28)



| | Definition | HTC, W/m²/K | Temp, °C |
|---|---|---|---|
| 1 | Top land | - | - |
| 2 | Groove top flank (1st comp. ring) | 900 | 185 |
| 3 | Groove root (1st comp. ring) | 150 | 175 |
| 4 | Groove bottom flank (1st comp. ring) | 4500 | 165 |
| 5 | 2nd land | 3000 | 165 |
| 6 | Groove top flank (2nd comp. ring) | 1000 | 155 |
| 7 | Groove root (2nd comp. ring) | 150 | 150 |
| 8 | Groove bottom flank (2nd comp. ring) | 3500 | 145 |
| 9 | 3rd land | 3000 | 145 |
| 10 | Groove top flank (oil ring) | 2000 | 135 |
| 11 | Groove root (oil ring) | 150 | 130 |
| 12 | Groove bottom flank (oil ring) | 2000 | 130 |

Figure - 28. Ring belt's boundary conditions

**Temperature field of the Z-engine's piston**

The material of the piston used is heat-treated steel 42CrMo4 [3, 13], which has a thermal conductivity of $k_{pist}$=42 W/m/K. The obtained temperature field of the piston is shown on figure 29 a.

The maximum combustion chamber temperature is 386 $^0$C. The maximum temperature in the ring belt zone is 272 $^0$C.

If we switch off oil supply and change BCs in oil gallery to free air convection ($HTC_g = HTC_{air}$) the temperature field of piston will change (figure 29 b.) The maximum combustion chamber temperature becomes 422 $^0$C and temperature in the ring belt zone reaches 312 $^0$C.



Temperature
Unit: $^0$C

390.87 Max
360.98
331.1
301.21
271.32
241.44
211.55
181.66
151.78
121.89 Min

428.75 Max
394.76
360.77
326.78
292.78
258.79
224.8
190.81
156.82
122.83

a)                                                                                                  b)
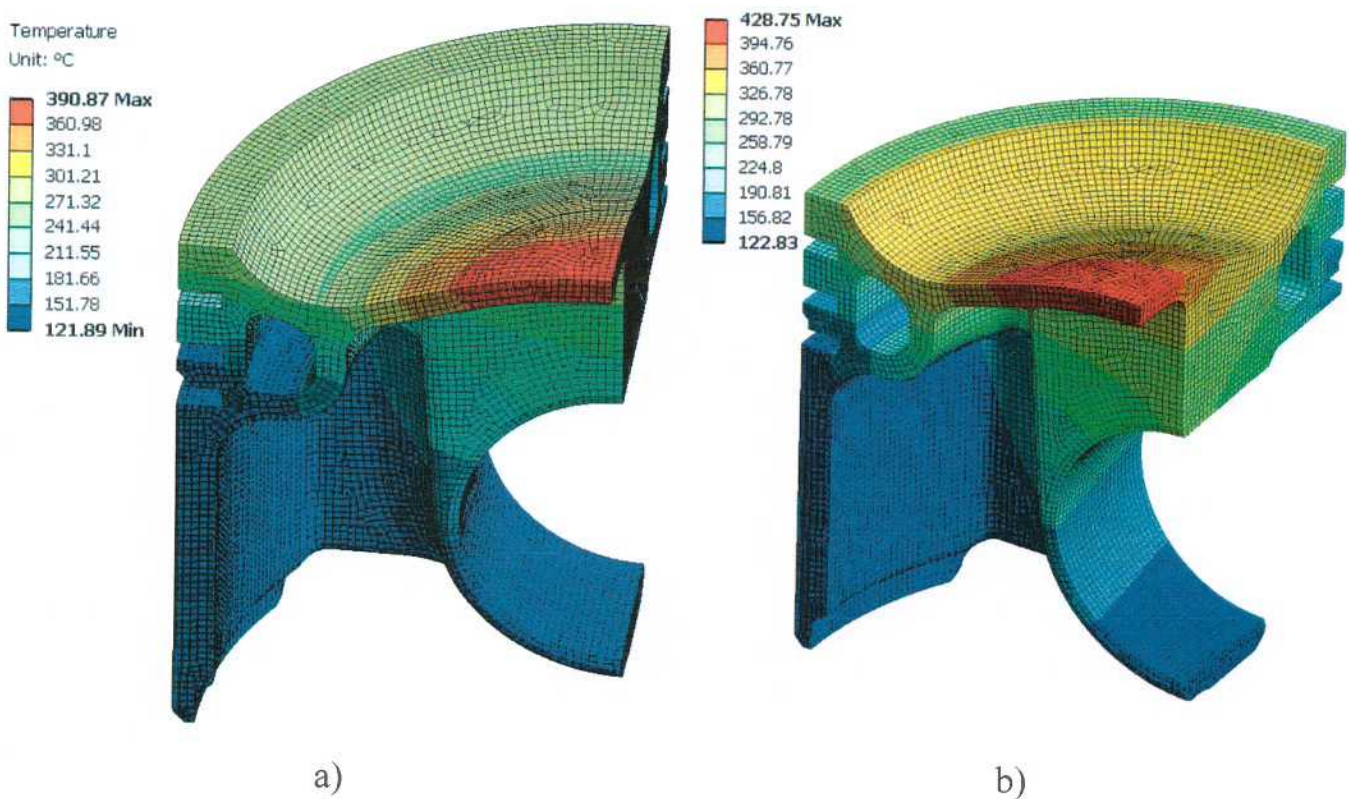
Figure - 29. Piston's temperature:

a) - the cooled case; b) the uncooled case

Distribution of temperature by firing surface of piston for two cases is present on figure 30.

For diesel engine's piston it's important to place gallery directly under the circumference of the piston bowl because of the nonhomogenous mixture preparation and the corresponding nonuniform heat generation in the combustion chamber (fig. 31).
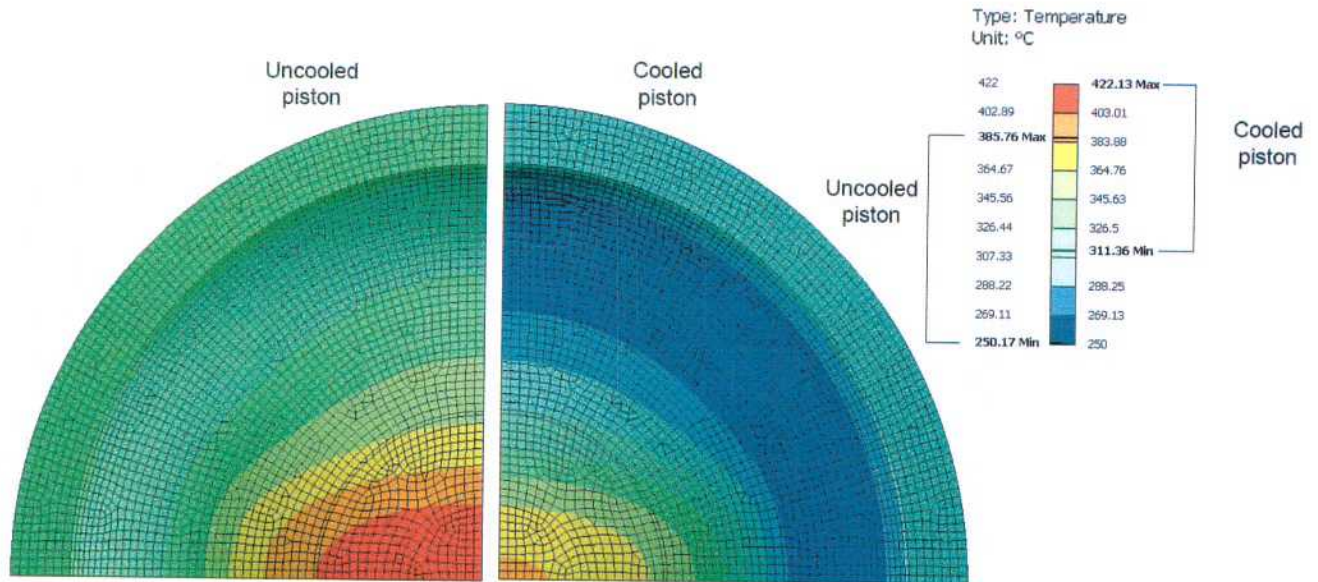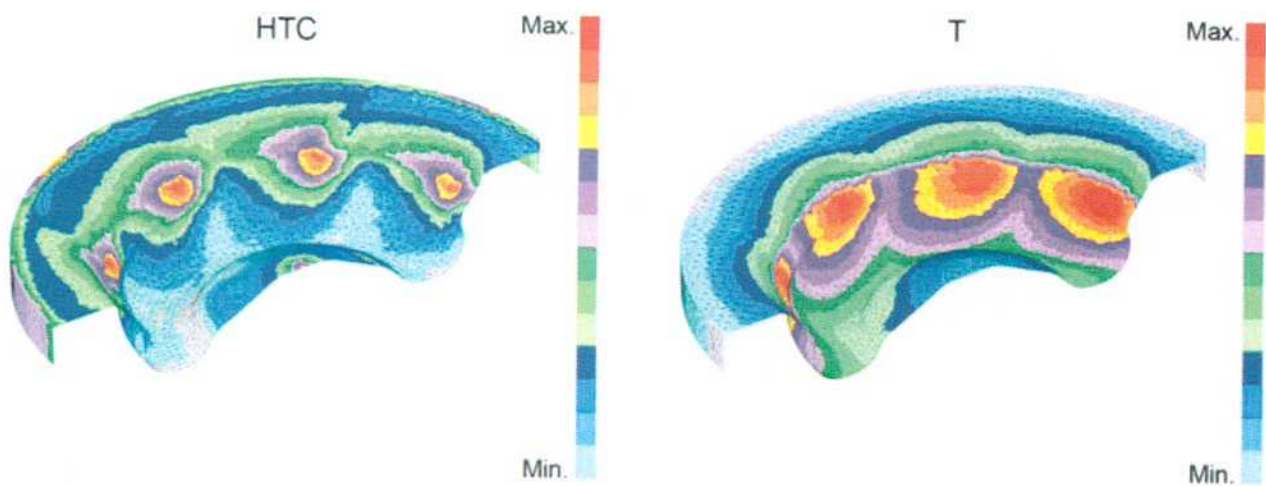
Figure - 30. The firing surface temperature



Figure - 31. Distribution of heat transfer coefficients (HTC, left) and gas temperature (T, right) on the piston crown of a commercial vehicle engine, from a CFD analysis [5]

Z-engine has enough uniform heat generation and HTC distribution along the radial direction of the piston (Table 2). In the same time there is no problem in the firing surface temperature however we need to decrease temperature in the ring belt zone.

In this case we can move gallery far away from combustion chamber bowl and in the same time move the ring belt zone down with increasing in compression and top land heights.

# III ) Re-design of the piston

## - Analysis of the piston's construction

We have two ways to decrease temperature in the ring belt zone:

- increasing top land height;

- optimization of cooling gallery shape.

From the compression height minimization point of view it is important to have the top land height as less as possible. The low compression height allows reducing the piston mass and the height of the engine. In the same time we will assume that the minimum thickness of the piston wall is 2.75mm due to machining limitations (I hope it's a enough reasonable value - I scale piston pictures from [3-4, 6, 13]).

Increasing in the top land height up to 9.5 mm leads to increase of the compression height from 35 mm to 39.5 mm (fig. 32). Further, it's possible to enlarge the top land height up to 11 mm without changing in the compression height.
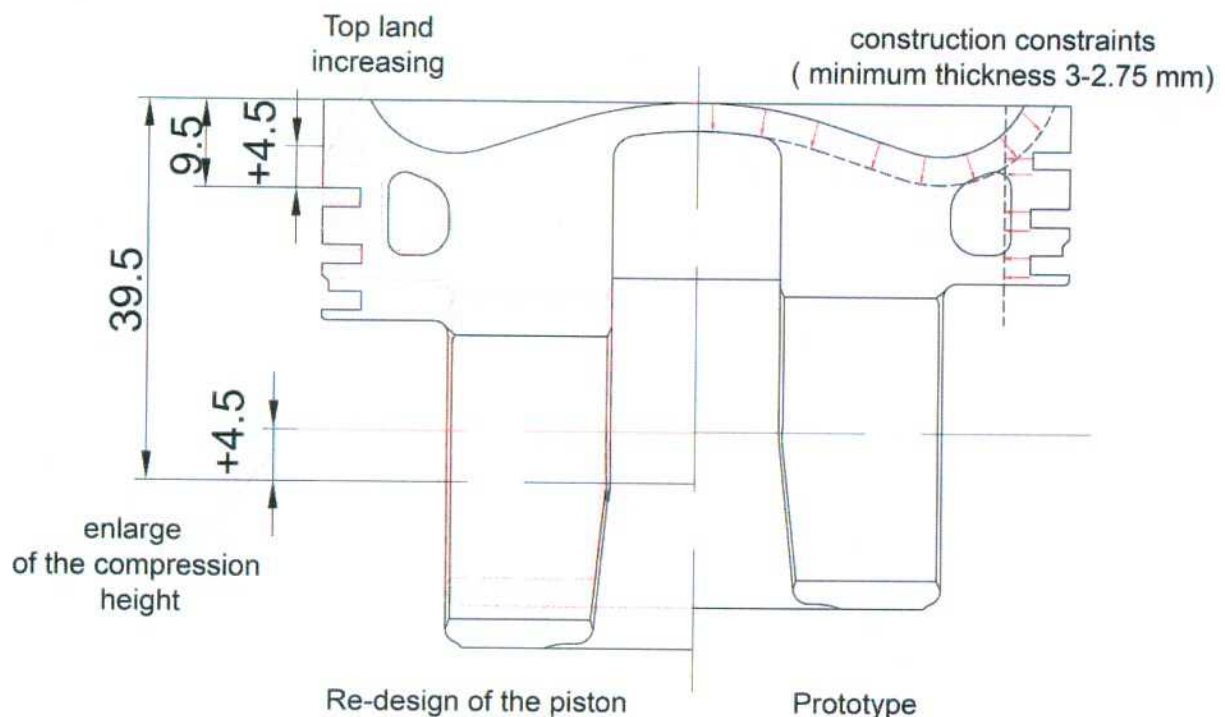


Figure - 32. First changing piston design

After temperature filed calculation we got the maximum temperature in the ring belt zone is 248 $^0$C instead of 272 $^0$C for previous piston design. However, there is no significant deformation in total heat flux vector lines (fig. 33). It means that the cooling gallery has no serious impact on temperature of the first ring top flank.
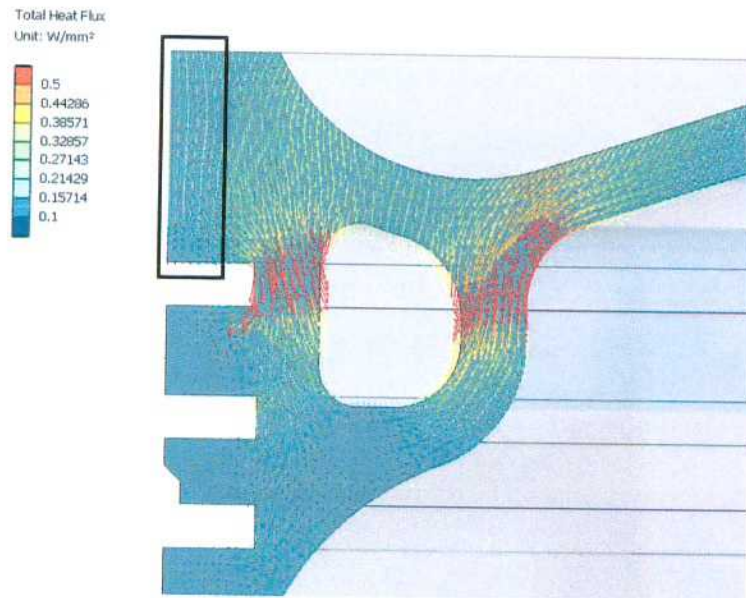
Figure - 33. Total heat flux vector's lines

If we move down top land of the first ring a bit we will be able to reshape the cooling gallery in the space between the 1st ring groove and combustion chamber bowl (fig. 34).
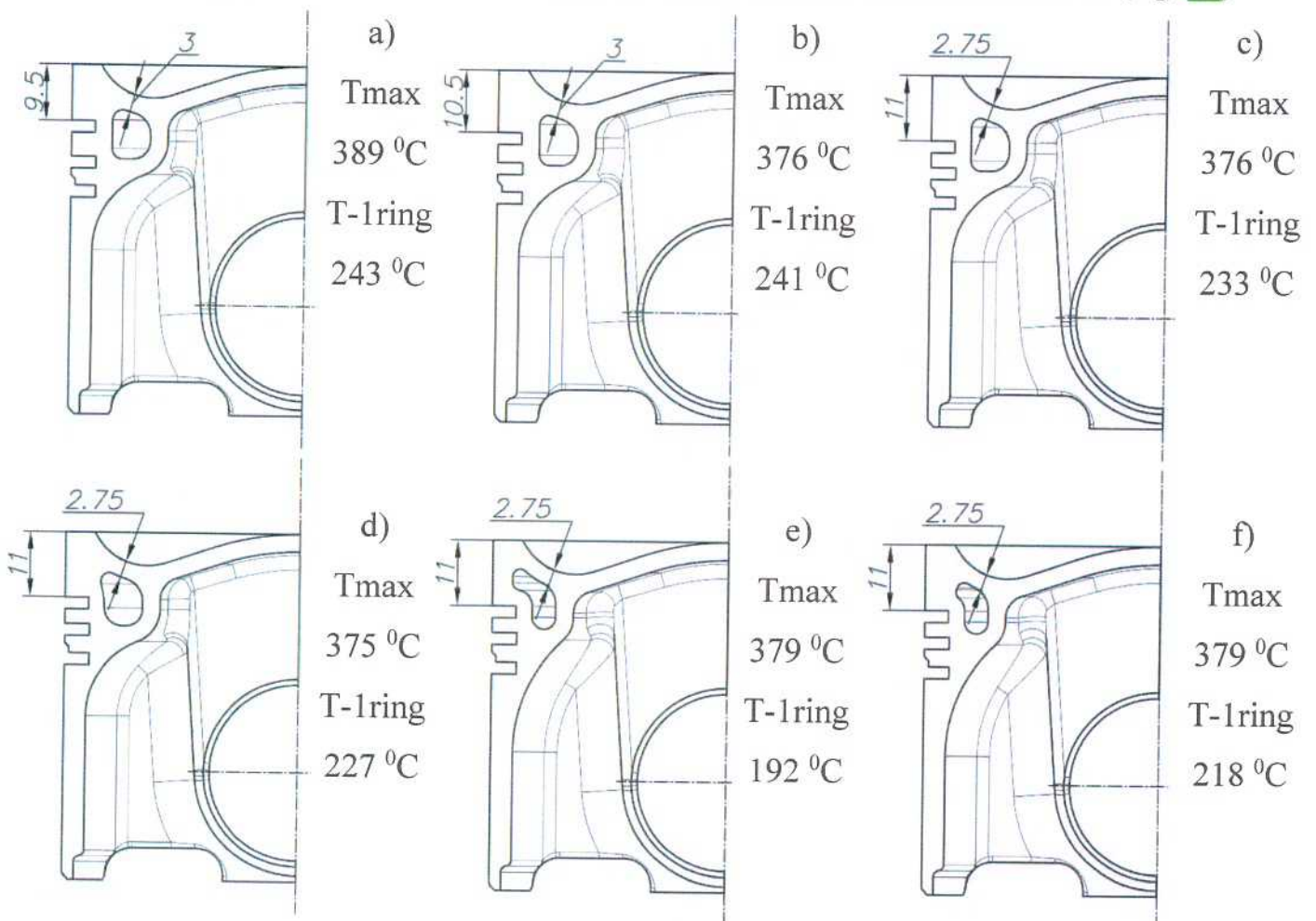


a)
Tmax
389 $^0$C
T-1ring
243 $^0$C

b)
Tmax
376 $^0$C
T-1ring
241 $^0$C

c)
Tmax
376 $^0$C
T-1ring
233 $^0$C

d)
Tmax
375 $^0$C
T-1ring
227 $^0$C

e)
Tmax
379 $^0$C
T-1ring
192 $^0$C

f)
Tmax
379 $^0$C
T-1ring
218 $^0$C

Figure - 34. Results of piston temperature calculation for different design

The resulting temperature field for the case 'f' is shown on figure 35. The maximum combustion chamber temperature is 382 °C. The average combustion chamber temperature is 290 °C.
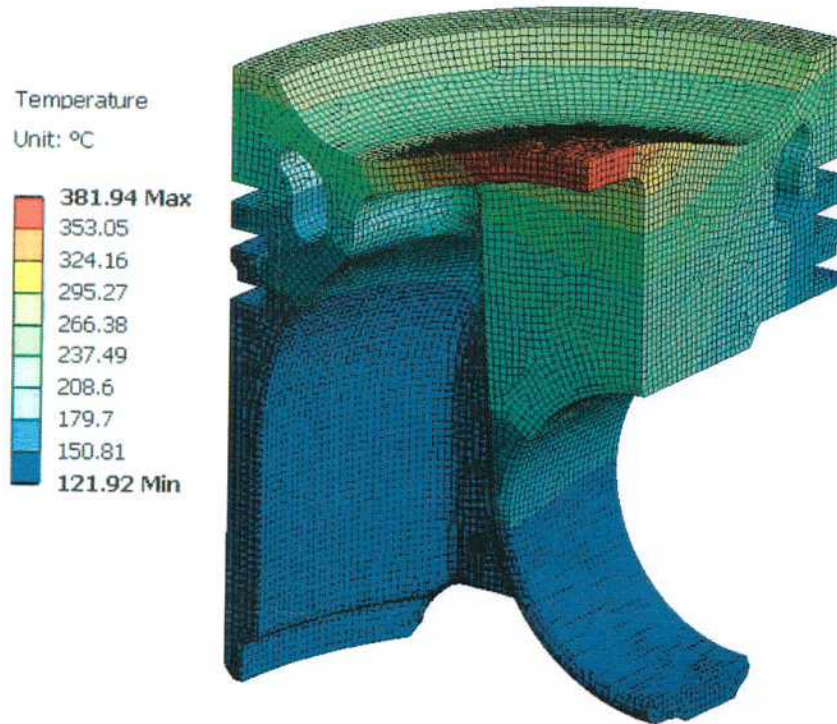


Figure - 35. Piston's temperature

The important part of piston design process is achieved reasonable weight. About 80% of the piston mass is located in the area from the center of the piston pin to the upper edge of the crown. The remaining 20% is in the area from the center of the piston pin to the end of the skirt. As mentioned early the compression height has a great significance, because it predetermines about 80% of the piston mass [5].

Piston mass $M_{piston}$ can be compared (without piston rings and piston pin) when related to the comparative volume $D^3$ [5, 15]. Today the piston's manufacturers try to achieve the same weight with steel as with today's aluminum alloys. In paper [13] the weight of aluminum and steel piston for Mercedes-Benz OM642 V6 diesel engine were compared, the difference became 52 grams. It means that we can use data from [5] to compare our results.

The density of 42CrMo4 is 7.7 g/cm³ [13]. The weight of base design of piston is 662 gram, the mass of modified piston is 770 gram (fig. 36).
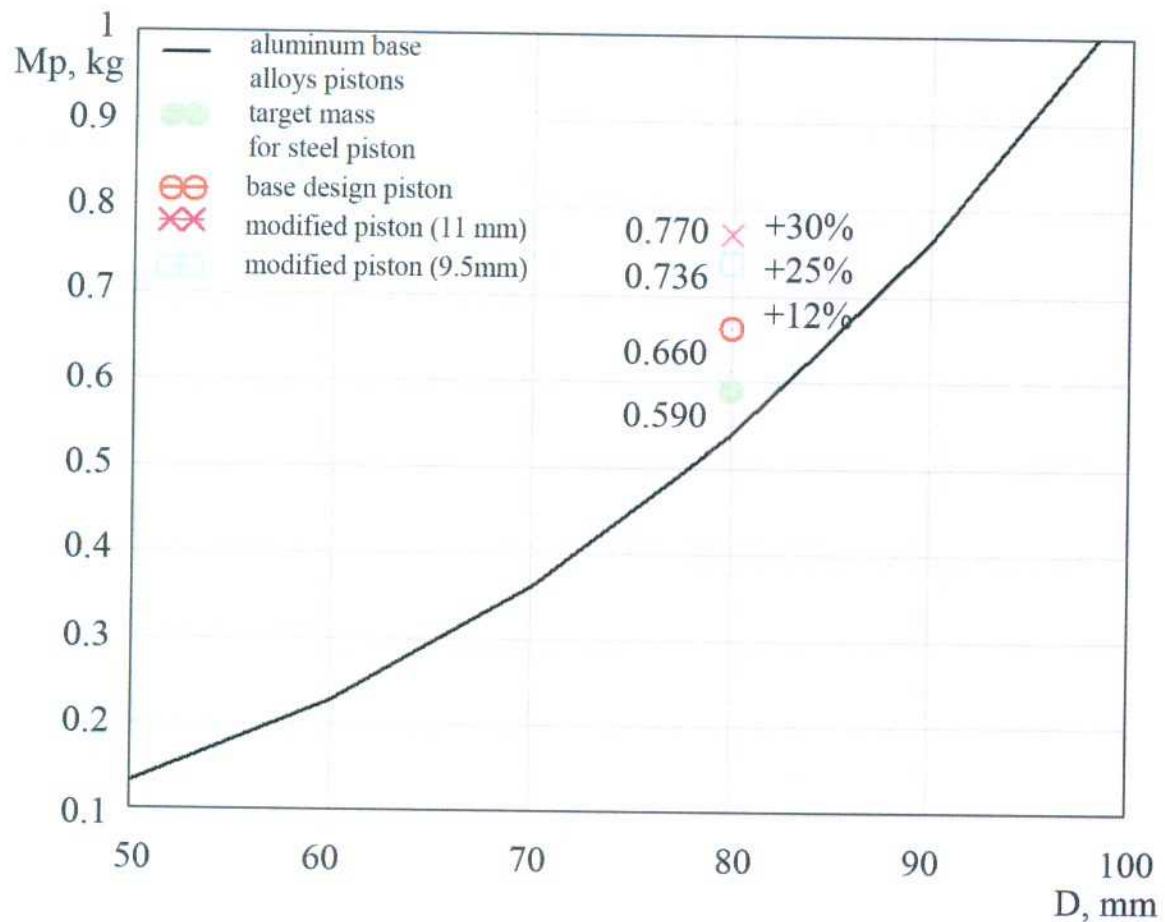
Figure - 36. Piston mass $M_{piston}$ (without piston rings and piston pin) for passenger car engines, as a function of the piston diameter

In [5] there is information for typical temperature maxima on the piston. The values shown on figure 37 are not a recommendation for limit values, but are simply orientation points for maximum measured values in current, highly stressed engines [5].

| Measurement point | Application | | | |
|---|---|---|---|---|
| | Commercial vehicle application | | Passenger car application | |
| | Al piston | Steel piston | Diesel engine | Gasoline engine |
| Bowl rim | 340°C | 470°C | 380°C | – |
| Piston crown | – | – | – | 290°C |
| 1st piston ring groove | 260°C | 260°C | 300°C | 270°C |
| Pin boss | 190°C | 180°C | 235°C | 240°C |

Figure - 37. Measured maximum temperatures on the piston for different applications [5]

This data agrees with results in papers [3 and 13] (fig. 38).

a                                                                                      b
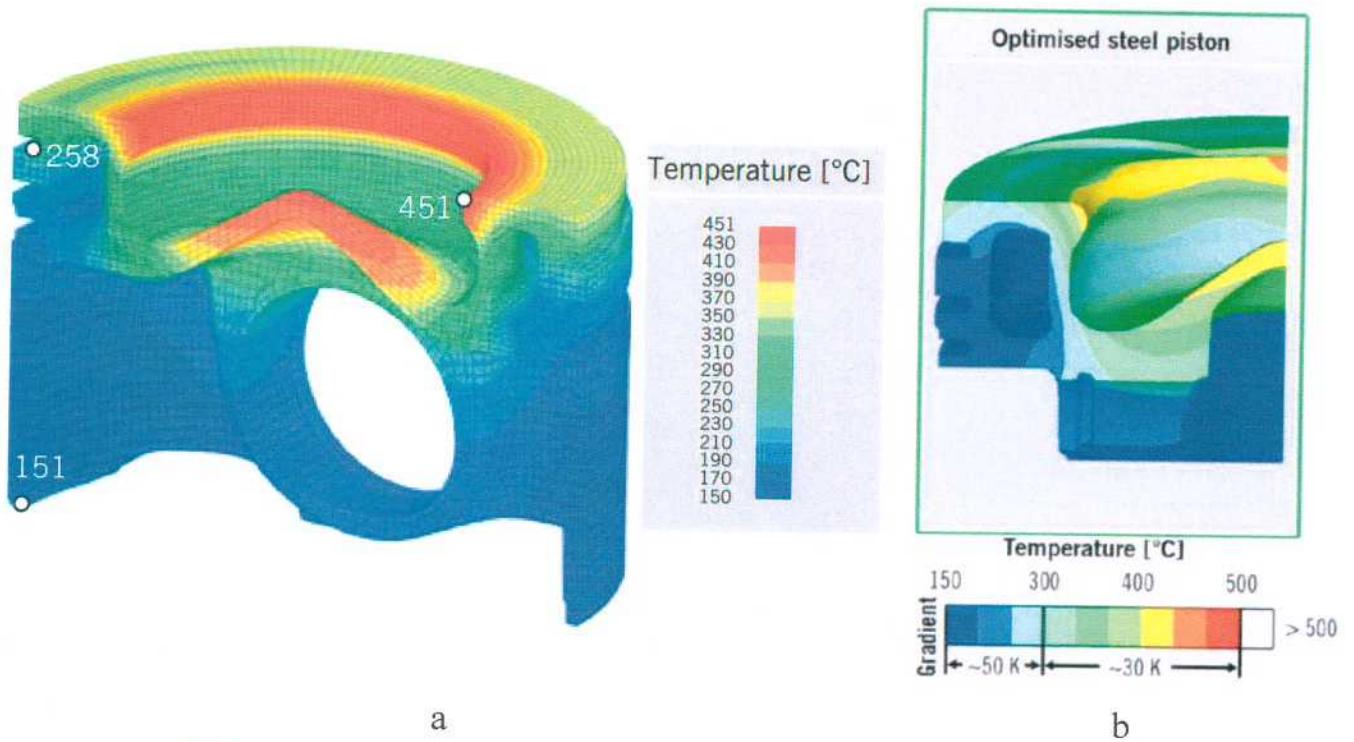
Figure - 38. Temperature profile between the piston bowl and the cooling gallery:

a) - [3], b) - [13]

If we reduce top land distance up to 9.5 mm (fig. 34 - case 'a') we will get temperature in first ring groove is equal to 243 $^0$C and mass of the piston is 736 gram (fig. 36).

I guess that the difference in weight of original steel piston and our design might be explain by shape of combustion chamber. In comparing with shallow combustion bowl, the deep bowl allows to reduce mass in under the crown space (fig. 39)
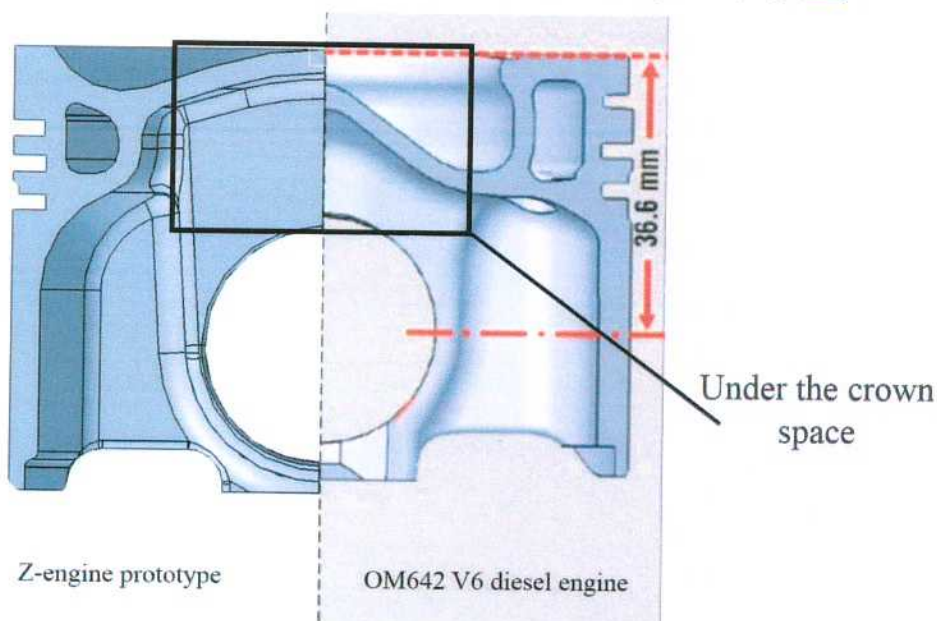


Figure - 39. Comparing of pistons

Nevertheless the increasing in mass can be compensating by relatively low engine speed compare with traditional automotive diesel engine.

We have one more opportunity to reduce 1st ring groove temperature and weight of the piston it is to make the combustion chamber bowl narrower and deeper. In this case we will move 1st ring groove up to the top of the piston reducing the compression height and in the same time effectively using under the crown space. The narrow bowl allows placing the cooling gallery in gap between the bowl itself and the ring land. By it's not a good idea to change working process for improving piston design.

# IV) Refined boundary conditions for piston skirt and rings
## - Analysis of stress for the piston

For very highly stressed pistons and piston components, the chromium-molybdenum alloy of heat-treated steel 42CrMo4 is used[3, 5, 13]. It should be mentioned that S. Schneider et al.[16] reached temperature 500 $^0$C for the piston crown of the experimental engine, made from this steel. In addition to improved full hardenability, both alloying elements promote carbide formation, and molybdenum also increases strength at elevated temperatures. However, even for this steel, a decrease in strength toward the core area must be expected for very large heat-treatment cross sections or changes in cross section [5]. The mechanical and physical properties are shown in Table 3[5].

Table 3

| Description | | 42CrMo4 |
|---|---|---|
| 1. Tensile strength, $R_m$ [MPa] | 20°C | 920–980 |
| | 130°C | 870–960 |
| | 300°C | 850–930 |
| | 450°C | 630–690 |
| 2. Yield strength $R_{p0,2}$ [MPa] | 20°C | 740–860 |
| | 130°C | 700–800 |
| | 300°C | 680–750 |
| | 450°C | 520–580 |
| 3. Fatigue strength Tbw [MPa] | 20°C | 370–440 |
| | 130°C | 350–410 |
| | 300°C | 340–400 |
| | 450°C | 280–340 |
| 4. Young's modulus E [MPa] | 20°C | 212,000 |
| | 130°C | 203,000 |
| | 300°C | 193,000 |
| | 450°C | 180,000 |
| 5. Thermal conductivity $\lambda$ [W/mK] | 20°C | 44 |
| | 130°C | 43 |
| | 300°C | 40 |
| | 450°C | 37 |
| 6. Linear thermal expansion B [$10^{-6}$ m/mK] | 20–300°C | 13.2 |
| | 300–450°C | 13.7 |

**Heat and mechanical load of the piston**

1) Thermal loads:

The temperature distribution (fig. 35) is the cause of significant temperature gradients. The piston expands greatly in the hot areas, whereas expansion is less in the cooler areas. The thermal stresses thus induced—primarily compressive stresses—are greatest at the crown and bowl area, and can exceed the yield point of the piston material there.

2) Gas force:

The gas pressure is applied to the simulation model over the entire piston crown, down to the lower flank of the top ring groove. The maximum cylinder pressure is 235.7 bar;

3) Inertia force:

The oscillating motion of the piston in the cylinder generates accelerations (Fig.18). Acceleration reaches 1283 $m/(s^2)$ at 1500 RPM. In the FE model, the acceleration is applied globally to the piston and piston pin. The model is fixed in the axial direction at the connecting rod small end's contact surface.

4) Lateral force:

We need to consider this type of load mainly during optimization of the wear and profiling of the piston's skirt. It can be neglecting, because it reaches zero value - at TDC position of the piston when gas and inertia forces are maximum.

The FE model consists from the piston and the piston pin (fig. 40).
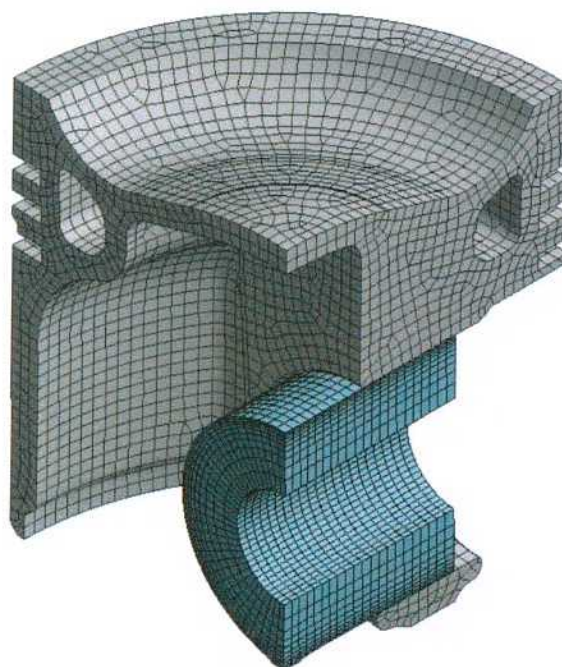


Figure - 40. FE model of the piston(25 thousand free hex-dominated mesh elements)

**Stresses due to temperature loading**

Figure 41, 42 shows the distribution of the thermally induced stresses in the piston. The temperatures on the piston crown generate compressive stresses in under the crown area and maximum tensile stresses at the edge of boss support area and under the crown area.
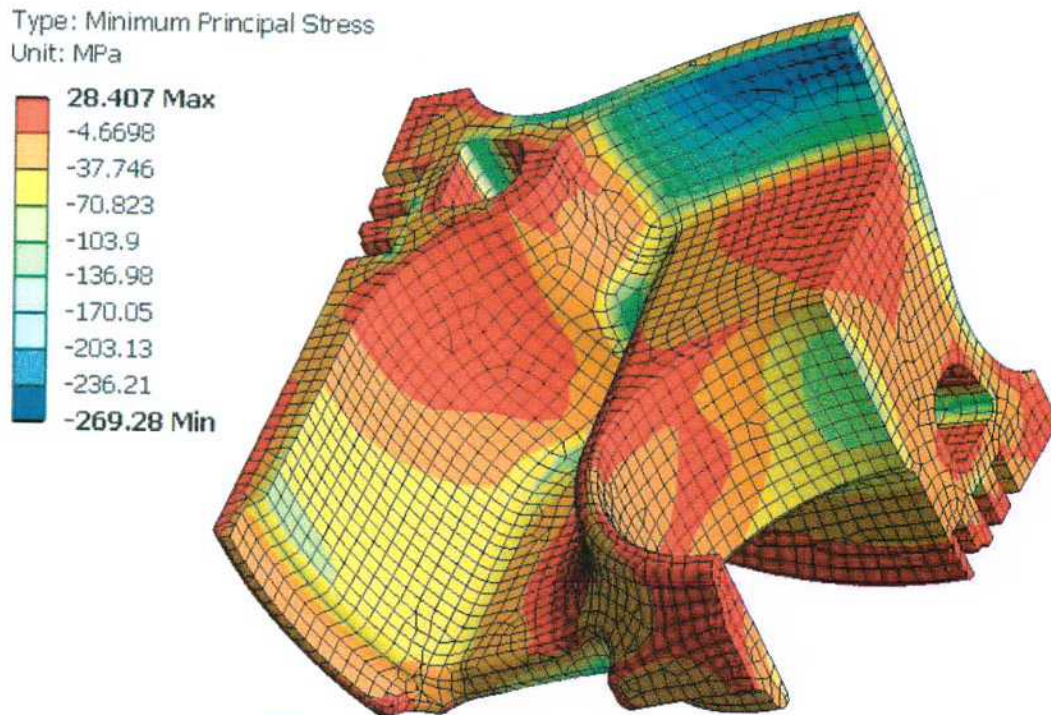


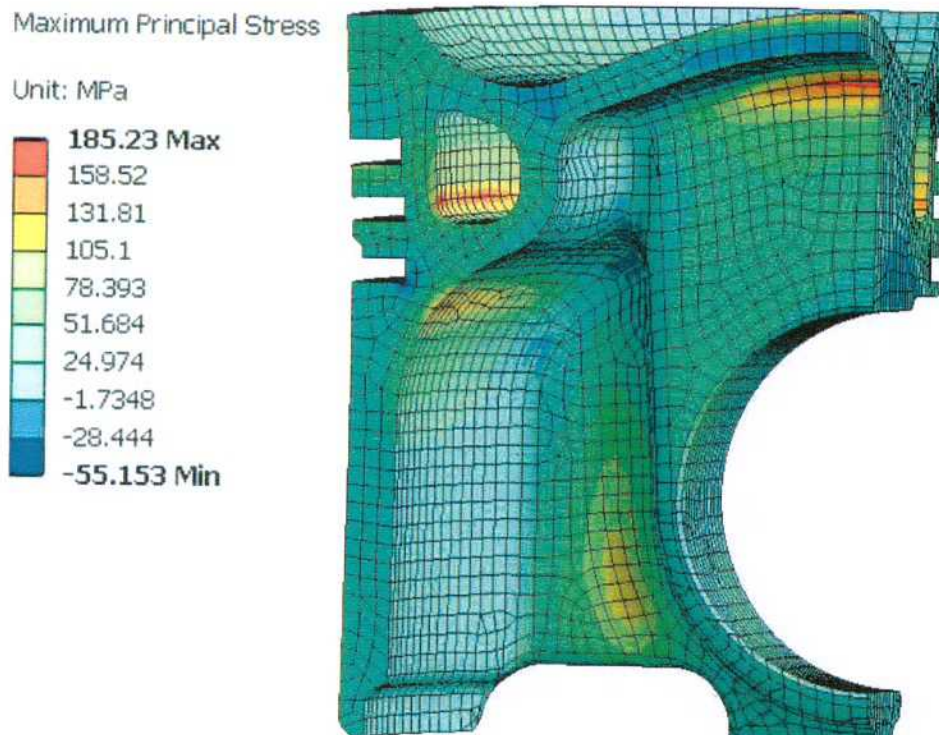Figure - 41. Minimum Principal Stress (Thermal load)



Figure - 42. Maximum Principal Stress (Thermal load)

**Stresses due to mechanical loading**

Under gas force load, the pin boss and support area and the transition of the support area into the piston crown are clearly loaded by compressive stresses (fig. 43).
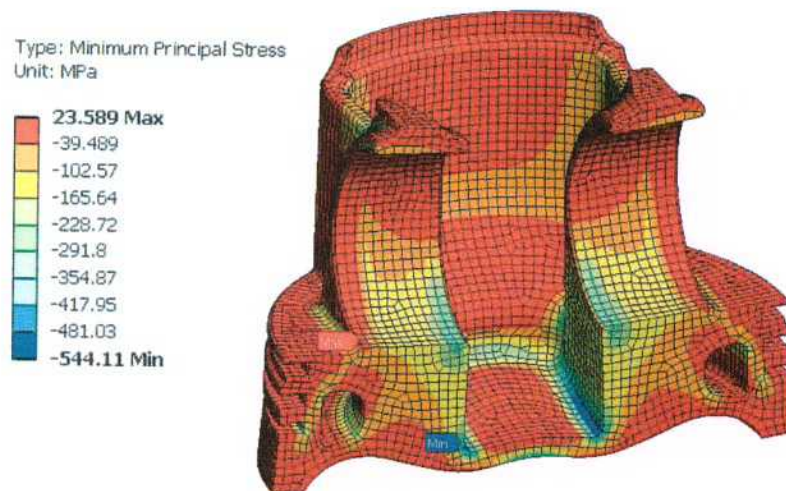


Figure - 43. Minimum Principal Stress (Mechanical load)

The largest deformation as expected was in the center of the combustion bowl (fig. 44). If it need we will be able to increase a wall thickness later.
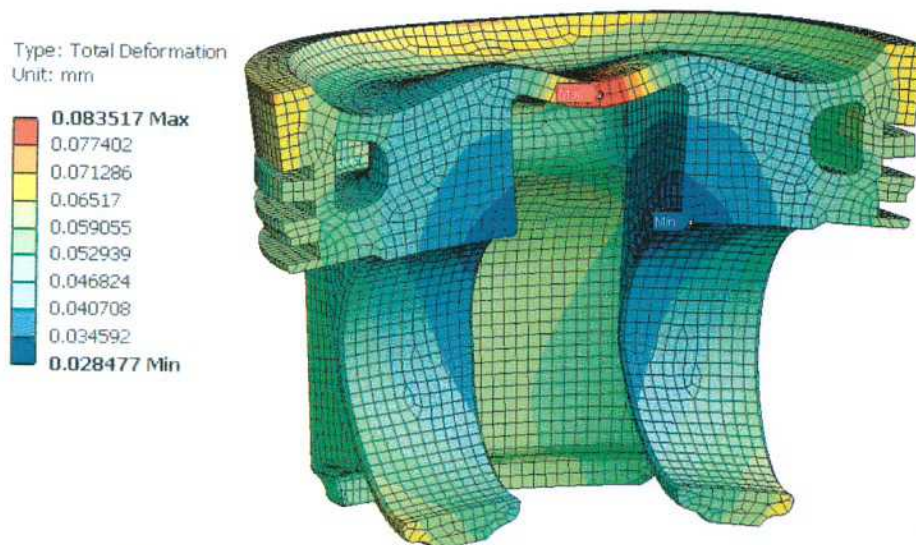


Figure - 44. Total deformations (Mechanical load) - scale 100:1

**Stresses due to complex loading**

For complex loading, the "temperature" load case, assumed to be quasi-static, is superimposed in order to calculate the correct resulting stresses in the piston analysis.

The piston is deformed "around the piston pin." This deformation generates stresses induced by the gas force in addition to the temperature stresses (fig. 45).

Type: Total Deformation
Unit: mm

0.18978 Max
0.17034
0.1509
0.13146
0.11201
0.092573
0.073132
0.053691
0.03425
0.014809 Min
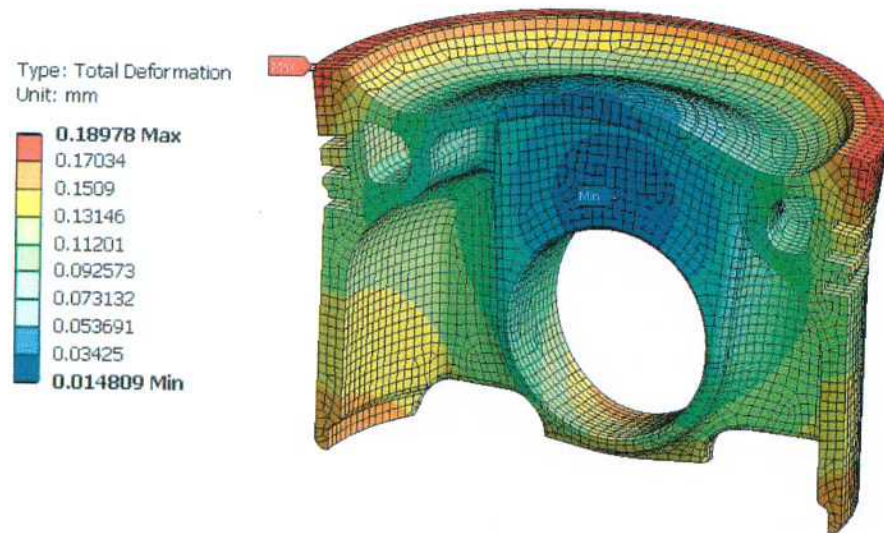
Figure - 45. Total deformations (complex load)- scale 25:1

The maximum of stress is in the same places as for "mechanical loading" (Fig. 46-47) but the maximum deformations corresponding with "temperature loading". We can decrease level of stress at the edge of boss support area making filled radius is greater.
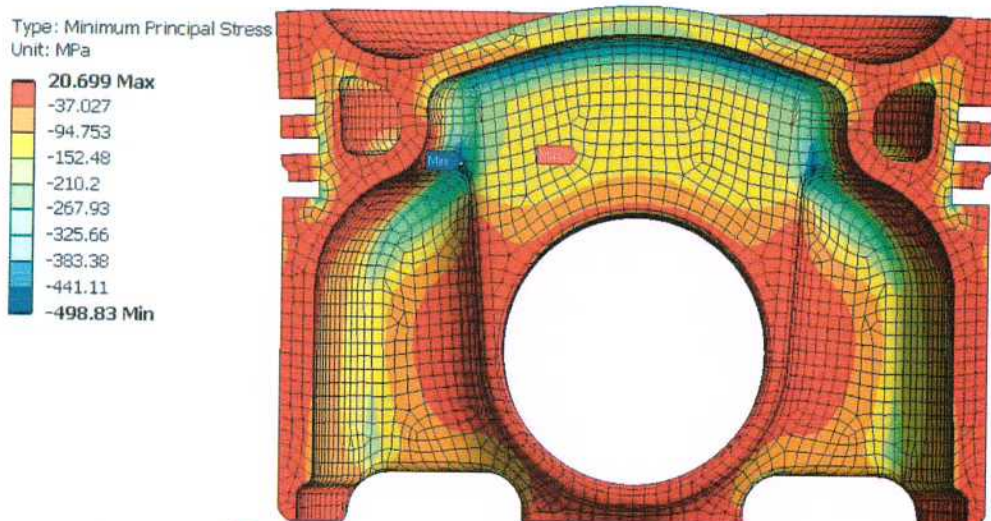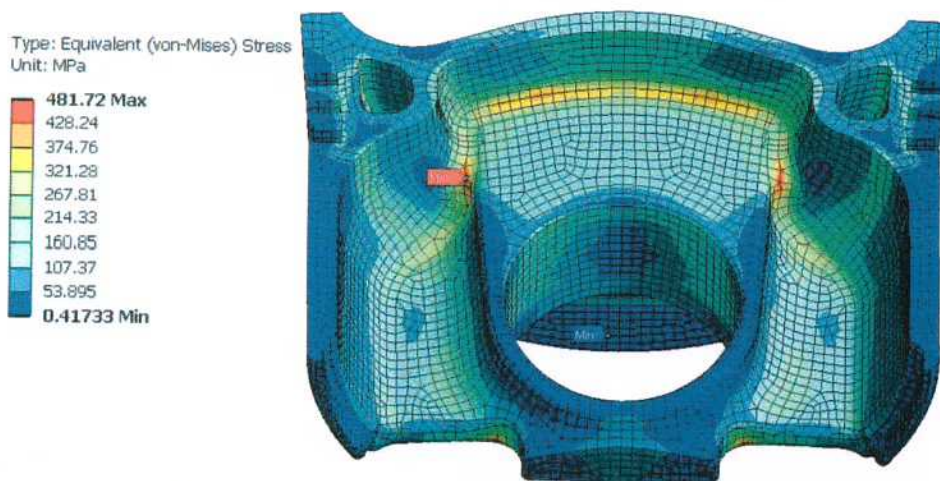


Type: Minimum Principal Stress
Unit: MPa

20.699 Max
-37.027
-94.753
-152.48
-210.2
-267.93
-325.66
-383.38
-441.11
-498.83 Min

Figure - 46. Minimum Principal Stress (complex load)



Type: Equivalent (von-Mises) Stress
Unit: MPa

481.72 Max
428.24
374.76
321.28
267.81
214.33
160.85
107.37
53.895
0.41733 Min

Figure - 47. Equivalent (von-Mises) Stress(complex load)

However, from the present results point of view the yield point hasn't been exceeded (table №3). It's a good enough result.

Further thermal fatigue analysis [17] should be conducted but it's really complicated task, and I think it's no necessary now.

For refining boundary conditions for piston skirt and rings we have to know the clearance of the piston in hot state. It means that the profile of piston contact surface should be set and some iterative simulations performed for evaluate the gap during working process. After the calculation of stress we get radial deformations of the piston (Fig. 48).
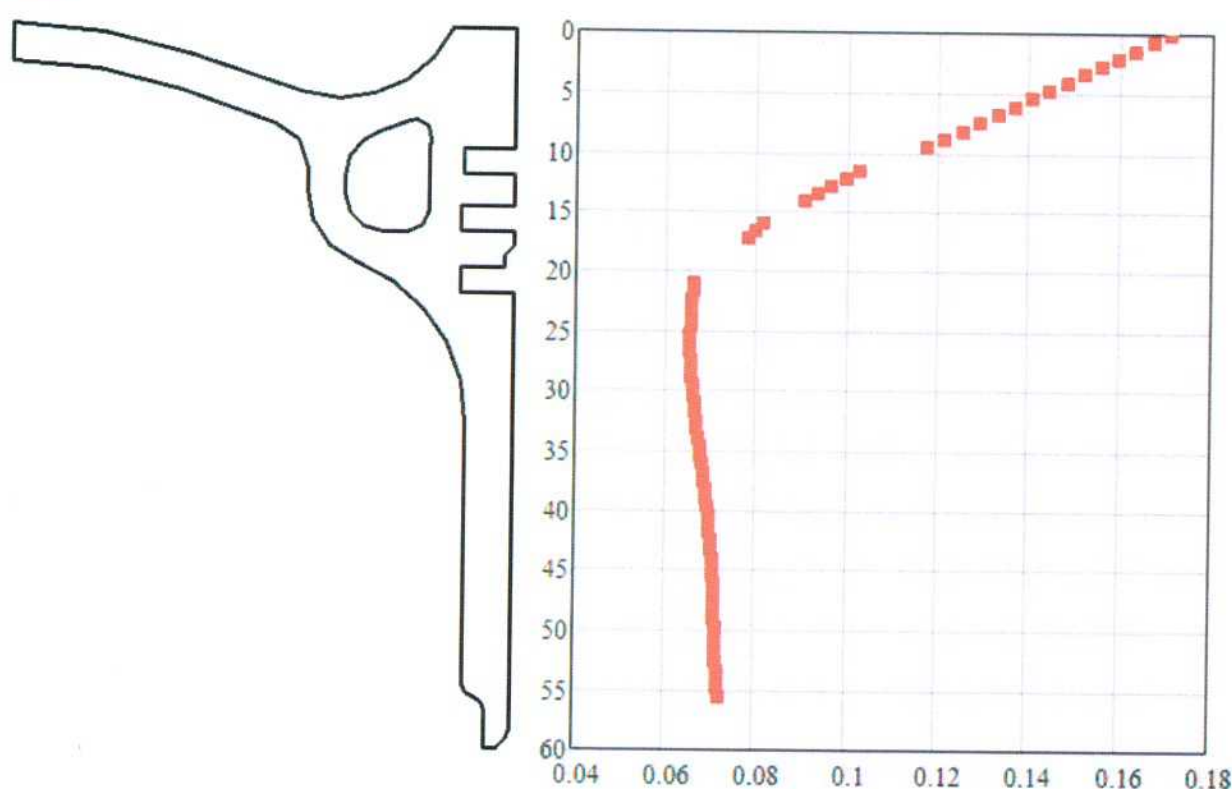


Figure - 48. Radial deformation of the piston

These results can be comparing with data of the D. Gabriel and T. Hettich paper [18].

The deformation in top land zone has the similar behavior (Fig. 49). The greater gap in this area compensates for the great thermal expansion due to high temperatures in this area and for the deformation due to gas pressure. For noise-sensitive engines, in particular, there should be no contact here between the piston and the cylinder liner (Fig. 50).
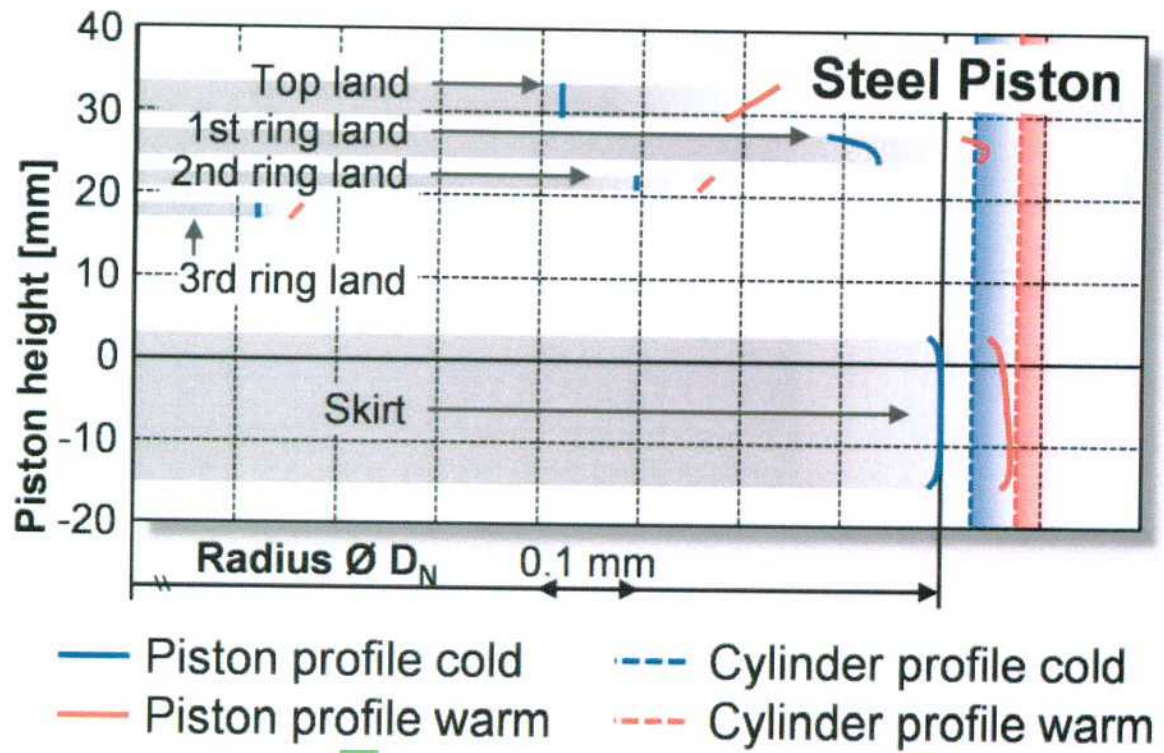
Figure - 49. Installation clearance cold/warm [18]

We choose the following dimensions for piston skirt and ring belt region (fig. 50) according to the results of FEA simulations and data from [18].
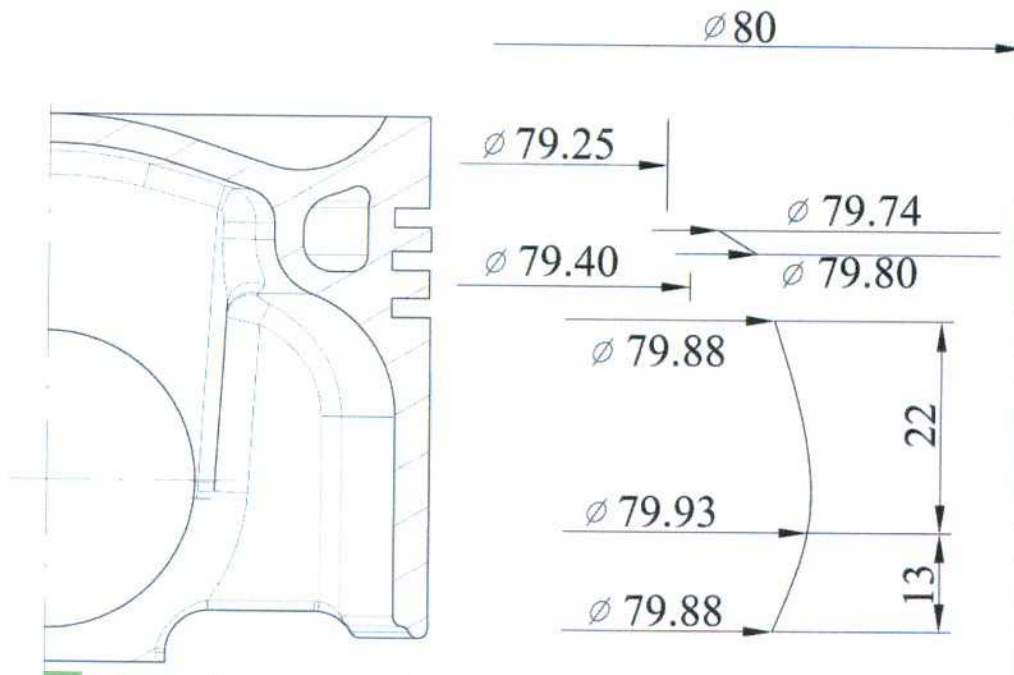


Figure - 50. The estimated mantle curve in thrust/antithrust direction (cold case)

The cylinder liner for Z-engine was chosen based on Mercedes-Benz concept [19]. Aluminum alloy AlSi12MgCuNi (MAHLE 124V [20]) is used as materials and dimensions were collected from available data [19] - figure 51. The mechanical and physical properties of aluminum alloy are shown in Table 4[20].
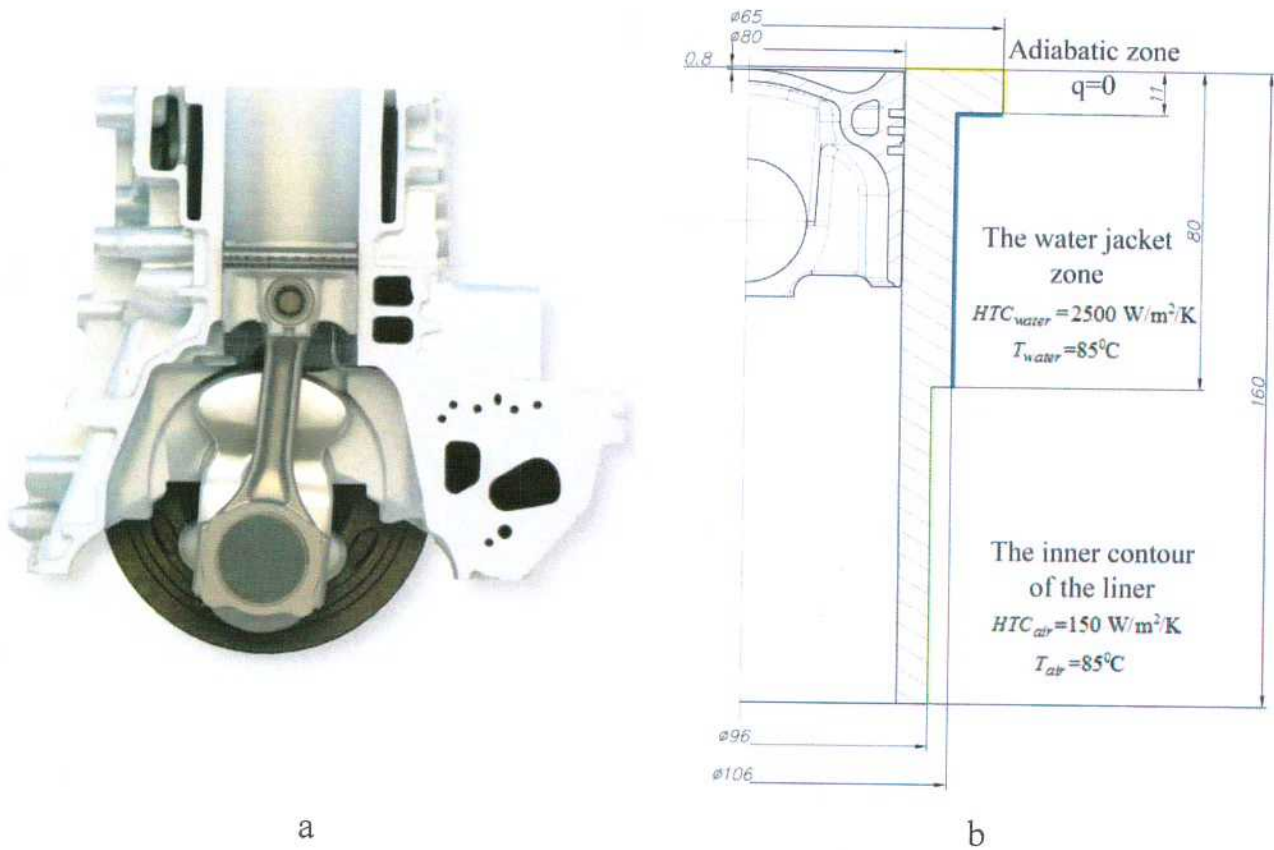
Figure - 51. The cylinder's liner design :

a) The Mercedes-Benz OM 654- [19], b) - sketch for Z-engine

Table 4

| Description | | AlSi12MgCuNi |
|---|---|---|
| 1. Tensile strength, $R_m$ [MPa] | 20°C | 210-230 |
| | 150°C | 180-200 |
| 2. Yield strength $R_{p0,2}$ [MPa] | 20°C | 190-210 |
| | 150°C | 170-180 |
| 3. Fatigue strength Tbw [MPa] | 20°C | 90-100 |
| | 150°C | 75-80 |
| 4. Young's modulus E [MPa] | 20°C | 80000 |
| | 150°C | 77000 |
| 5. Thermal conductivity λ [W/mK] | 20°C | 155 |
| | 130°C | 156 |
| 6. Linear thermal expansion B [$10^{-6}$ m/mK] | 20–100°C | 19.5 |
| | 100–200°C | 20.6 |

Depending on the required service life and operational reliability, various running surface coatings are available to the user of light-alloy cylinders [20]. The Mercedes-Benz

uses Nanoslide® technology. Nanoslide® is an innovative and economical technology designed to reduce the fuel consumption and $CO_2$ emissions of internal combustion engines. An extremely thin, low-friction coating is applied to the inner surfaces of the cylinders in an aluminum engine block. As up to 25 percent of the energy in fuel is used to overcome in-engine friction, particularly at part load, fuel savings of several percent are attainable [21].

Twin-wire arc spraying (TWAS) is used to apply an extremely thin coating based on an iron-carbon alloy to the inner surfaces of the cylinders in aluminium engine blocks. This produces a nano to ultra-fine, highly wear-resistant material structure with microporosity. This microporosity ensures effective lubrication in operation. It means that the heavy cast-iron liners measuring several millimetres in thickness can be replaced in aluminium cylinder blocks. The result is a mirror-smooth surface, with friction between piston, piston rings and cylinder wall reduced by up to 50 percent and weight savings of several kilograms [21].

During heat transfer calculations we have to take into account the thickness of this layer which equals to 0.1-0.2 mm. The equivalent thermal conductivity of the liner was calculated base on composite wall idea (fig.52).
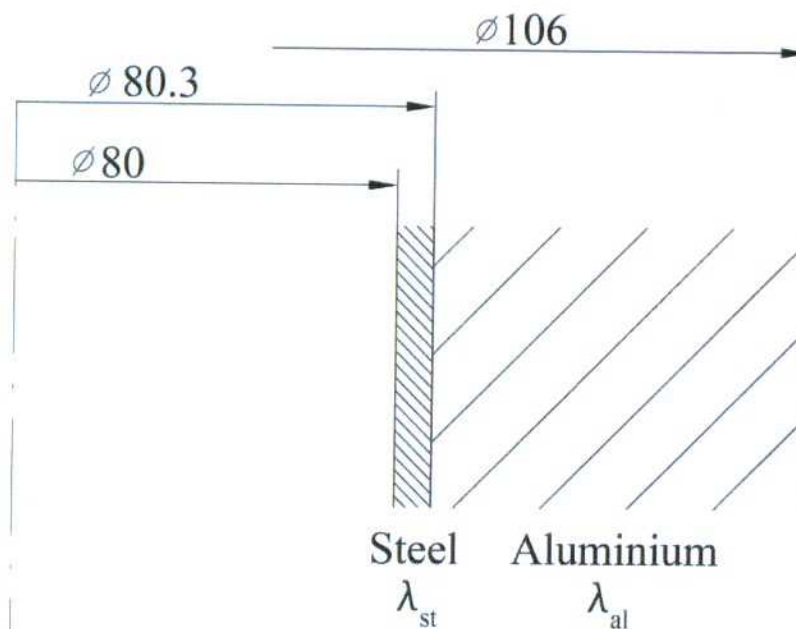


Figure - 52. Composite wall model for the cylinder liner

The effective thermal conductivity could be calculated using the following expression:

$$\lambda_{eq} = \frac{\sum\limits_{i=1}^{2} \ln \dfrac{D_{i+1}}{D_i}}{\sum\limits_{i=1}^{2} \dfrac{1}{\lambda_i} \ln \dfrac{D_{i+1}}{D_i}} \qquad (26)$$

According to Tables №2-№3 and geometry of cylinder liner, we got the $\lambda_{eq}$=151 W/m/K. In conclusion, it should be said that it's not a big different compare with aluminium.

For refining boundary conditions we have to know information about ring geometry and working conditions. Some of information I got from the paper of Harke et al [14] - figure 53. Most of data was reduced for Z-engine dimensions, but indeed I have no any more sources.

| | Serie | LFS | LF St |
|---|---|---|---|
| **1. Nut** | | | |
| |  |  |  |
| Ringtyp | HKBA | BA IF | BA IF |
| h1 x a1 [mm] | 2,5 x 3,1 | 2,0 x 2,9 | 2,0 x 2,9 |
| s1 [mm] | 0,31 | 0,31 | 0,31 |
| Tangentialkraft [N] | 13,1 | 10,0 | 10,0 |
| Oberflächenbehandlung | Chrom-Keramik | PVD | PVD |
| **2. Nut** | | | |
| |  |  |  |
| Ringtyp | M IFU | M IFU | M IFU |
| h1 x a1 [mm] | 2,0 x 3,2 | 1,5 x 2,9 | 2,0 x 2,9 |
| s1 [mm] | 0,7 | 0,5 | 0,5 |
| Tangentialkraft [N] | 9,9 | 7,6 | 9,2 |
| Oberflächenbehandlung | Mo Plasma | nitriert | nitriert |
| **3. Nut** | | | |
| |  |  |  |
| Ringtyp | DSF | DSF | DSF |
| h1 x a1 [mm] | 2,0 x 3,2 | 2,0 x 2,75 | 2,0 x 2,75 |
| s1 [mm] | 0,38 | 0,25 | 0,25 |
| Tangentialkraft [N] | 30,0 | 20,0 | 20,0 |
| Oberflächenbehandlung | Chrom | PVD | PVD |
| Gesamt-Tangentialkraft [N] | 53,0 | 37,6 | 39,2 |

Figure - 53. Ring's design (©Kolbenschmidt) [14]

Our department axisymmetric code was used for simulations. It's far far away from AVL EXCITE Piston&Rings possibilities but I need just heat boundary conditions and don't really want to minimize of piston slap induced noise or analyze cavitation and wear at the liners and oil consumption.

*Our program has the Russian language interface, and I don't think that it's necessary to show it here and translate. If you need this information, you could write me and I will do it.*

The minimum gap for piston skirt is 46.85 mkm. Refined boundary conditions are shown at figure 54.



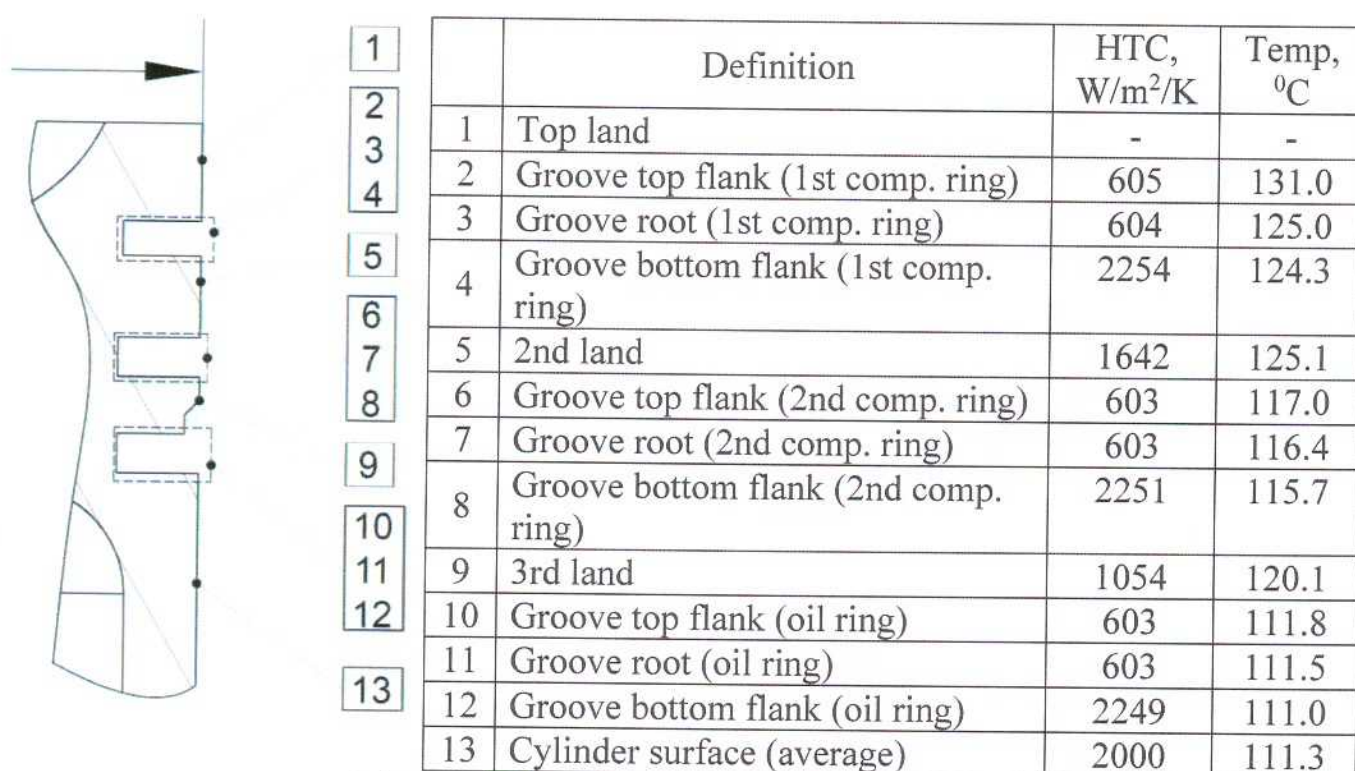| | | Definition | HTC, $W/m^2/K$ | Temp, $^0C$ |
|---|---|---|---|---|
| | 1 | Top land | - | - |
| | 2 | Groove top flank (1st comp. ring) | 605 | 131.0 |
| | 3 | Groove root (1st comp. ring) | 604 | 125.0 |
| | 4 | Groove bottom flank (1st comp. ring) | 2254 | 124.3 |
| | 5 | 2nd land | 1642 | 125.1 |
| | 6 | Groove top flank (2nd comp. ring) | 603 | 117.0 |
| | 7 | Groove root (2nd comp. ring) | 603 | 116.4 |
| | 8 | Groove bottom flank (2nd comp. ring) | 2251 | 115.7 |
| | 9 | 3rd land | 1054 | 120.1 |
| | 10 | Groove top flank (oil ring) | 603 | 111.8 |
| | 11 | Groove root (oil ring) | 603 | 111.5 |
| | 12 | Groove bottom flank (oil ring) | 2249 | 111.0 |
| | 13 | Cylinder surface (average) | 2000 | 111.3 |

Figure - 54. Ring belt's boundary conditions

It's should be mentioned that all the times rings lay down to bottom flanks of the grooves. I thing it's possible for our case because we have two-stroke cycle and big enough pressure even during exchanging phase. It means that for top flanks of grooves the heat transfer not very intensive and doesn't affect on the maximum temperature of the first ring groove.

The obtained temperature field after refining of boundary conditions is shown on figure 55. The maximum combustion chamber temperature is 389 $^0C$ (fig. 56). The maximum temperature in the ring belt zone is 232 $^0C$. The average combustion chamber temperature is 288 $^0C$.
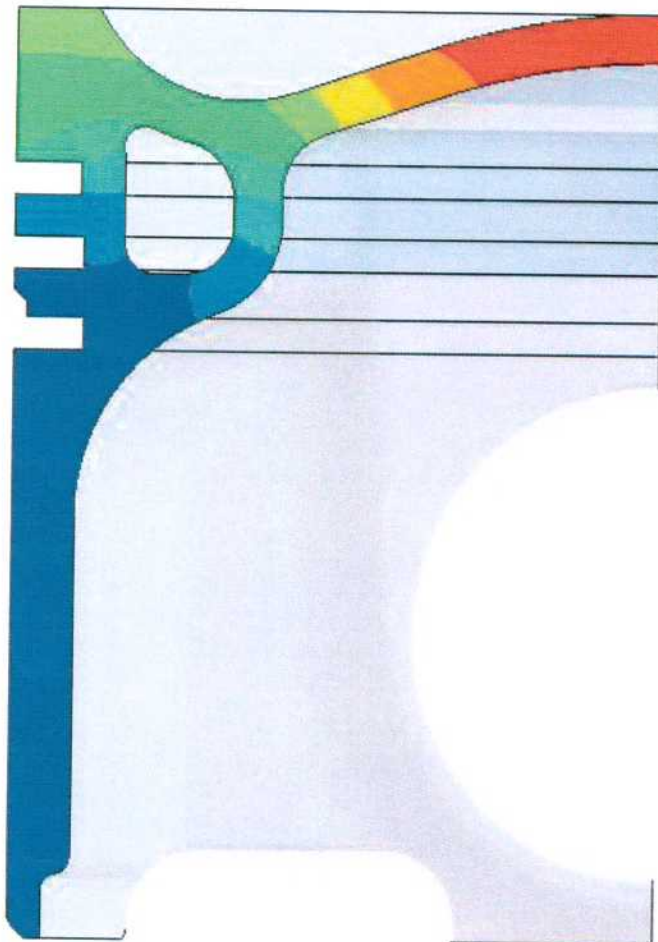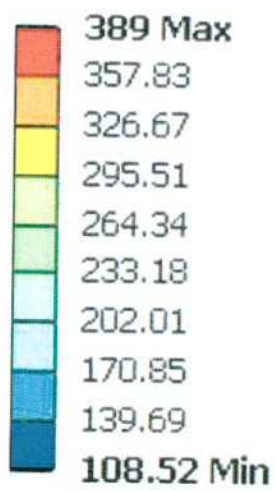
Type: Temperature
Unit: °C

389 Max
357.83
326.67
295.51
264.34
233.18
202.01
170.85
139.69
108.52 Min

Figure - 55. Piston's temperature (refined BC)



Type: Temperature
Unit: °C

389 Max
373.64
358.27
342.91
327.55
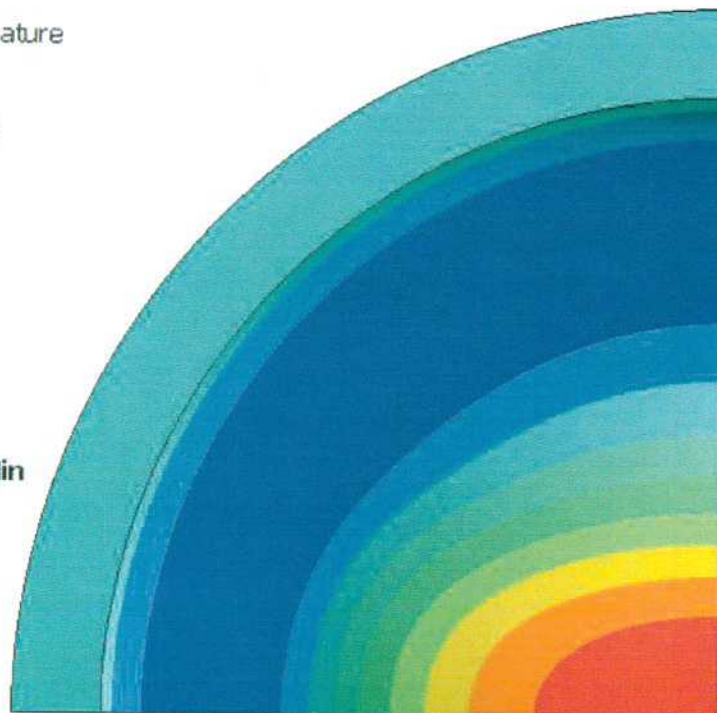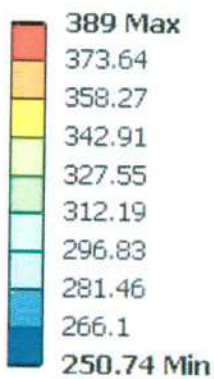312.19
296.83
281.46
266.1
250.74 Min

Figure - 56. The firing surface temperature (refined BC)

Calculations were provided for fig. 34 - case 'a' geometry. There is no different in maximum temperature, but the temperature of the 1-st ring top flank is less on 11 $^0$C.

The lower temperature in the ring belt zone cause by the temperature of the conjugate cylinder liner. This is result of high thermal conductivity of using aluminium alloy. Nevertheless we could bind the temperature error in the interval $\pm 5\%$ ($\pm 11$ $^0$C).

## V) The filling model validation

In this simulation we use simplify geometrical model without under the piston space - just a half of gallery volume (fig. 57).
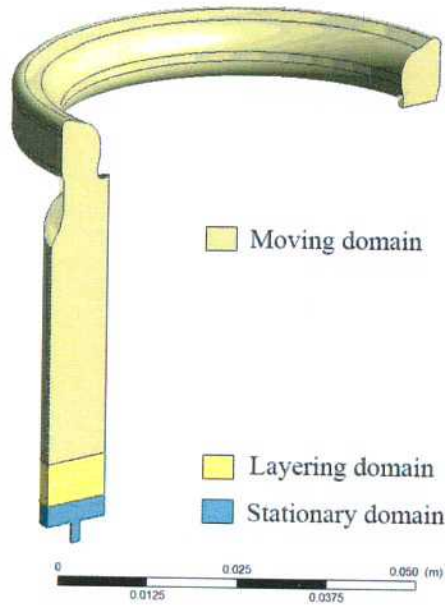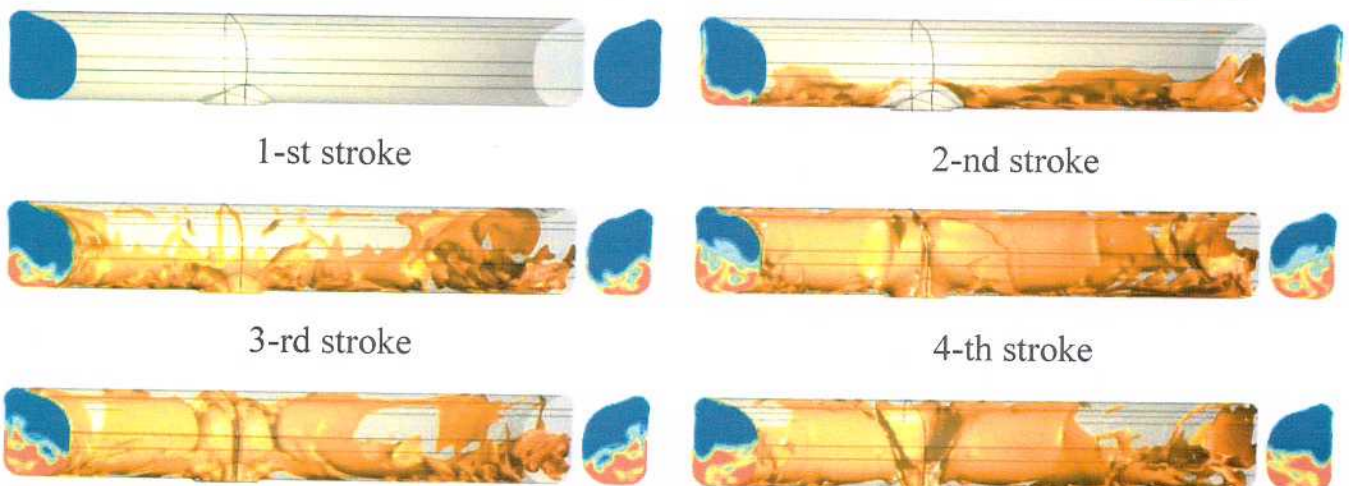


Figure - 57. The computational domain

There are following boundary conditions for present calculation and the oil volumetric flow rate 2.0 L/min:

- The oil supply velocity $V_{inlet}$ is 27.0 m/s (the oil supply pressure is 3 bar);

- The injector diameter $d_{inj}$ is 1.5mm;

Simulation was conducted for seventeen piston strokes. The total computation time was about 1.5 month. The timestep for explicit solver was about 1e-5 s for Courant number is equal to 5.

The oil filled ratio at the BDC point for different stroke is showed on the fig. 58.



1-st stroke

2-nd stroke

3-rd stroke

4-th stroke

5-th stroke      6-th stroke

7-th stroke      8-th stroke

9-th stroke      10-th stroke
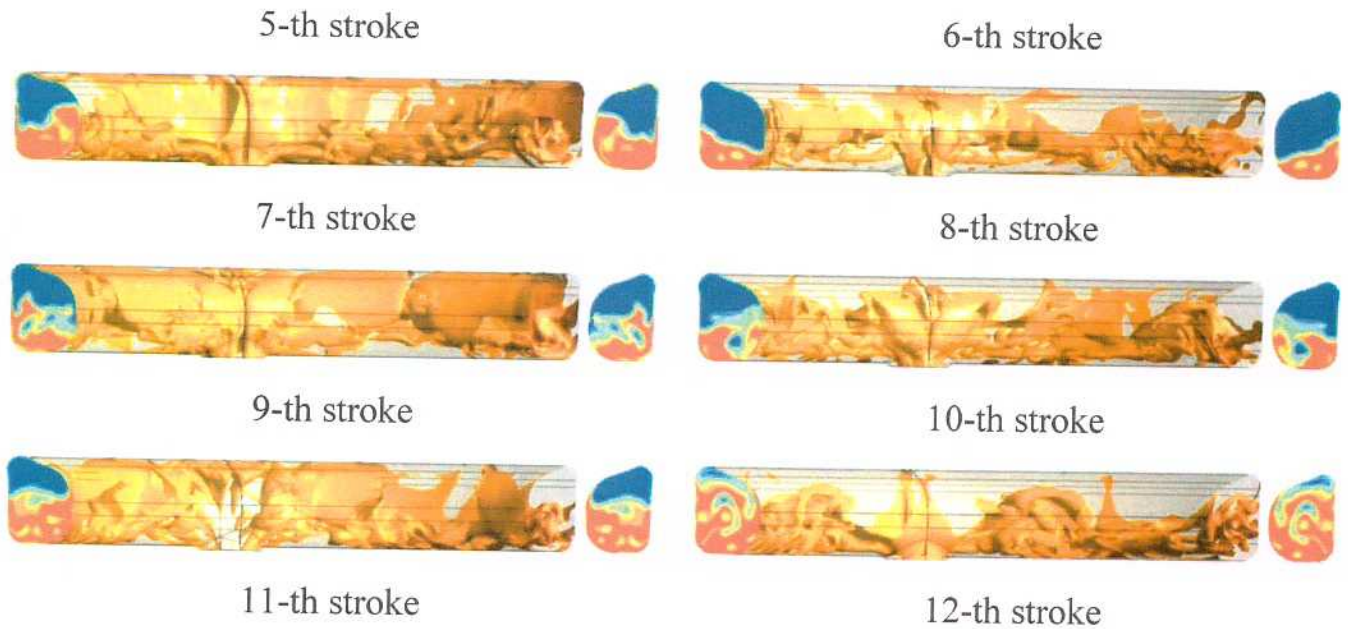
11-th stroke      12-th stroke

Figure - 58. The oil filled ratio at the BDC point

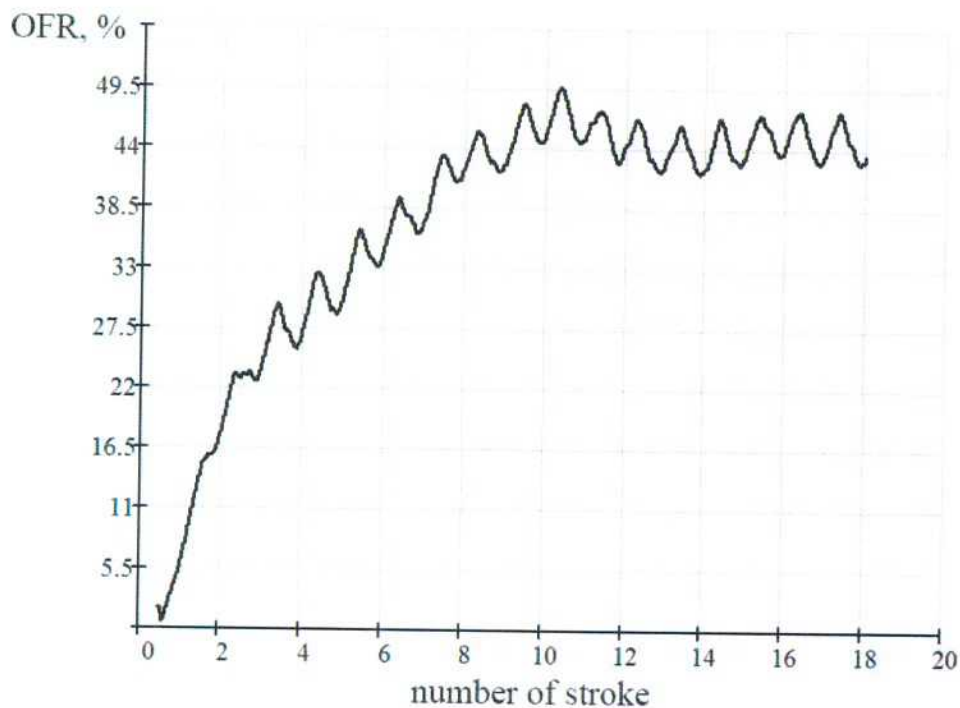The final filling curve is present on the figure 59.



Figure - 59. The oil fill ratio in respect of number of crankshaft revolution (CFD-modeling)

Corresponding to the described model (chapter III) one could see two stages of the filling process. At the first stage, then a piston is moving down to BDC point, oil is attached to top of gallery and didn't leave the cooling channel. On the other hand during the second stage oil left the gallery under the acceleration force. After the near ten/eleven

strokes the equilibrium between the flow rates of coolant coming in and going out of the cooling gallery is noticed.

The good agreement with CFD results was obtained using a discharge coefficient of cooling gallery outlet $\mu_{f\_out}$ 0.75 (4) - fig 60. The divergence in calculation is about 5-7 %.
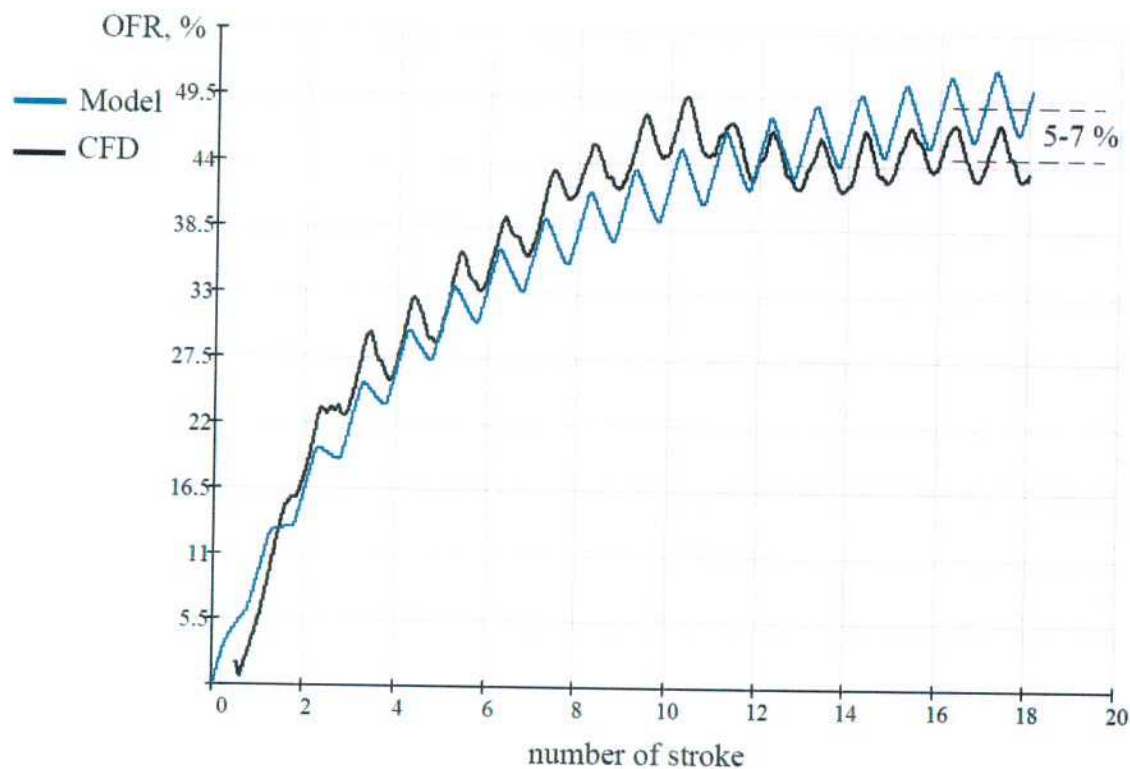


Figure - 60. The oil fill ratio in respect of number of crankshaft revolution (comparison)

The final characteristics of oil supply system are shown in Table 5.

Table 5

| Description | |
|---|---|
| The oil supply pressure, bar | 3.0 |
| The injector diameter $d_{inj}$, mm | 1.5 |
| The oil supply velocity $V_{inlet}$, m/s | 27.0 |
| Oil volumetric flow rate, L/min | 2.0 |
| Filling ratio, % | 45 |

# VI) Combined cooling of the piston

There are essentially two methods for feeding cooling oil to the piston. It can be fed to the cooling channel with nozzles mounted in the crankcase and supplies as a jet to the undercrown area [5]. For out case we will check using combined cooling system with two extra nozzles for spray jet cooling.

It is unobvious solution due to some geometrical restrictions already has existed in the construction:

- Area is being cooled by oil in gallery (fig 61a);

- Area is covered by piston pin (fig 61b);

- Crossing area with gallery's cooling jet (fig 61c);

- Area of a conrod excursion envelope (fig 61d). The conrod executes a swinging motion with each revolution of the crankshaft [22].
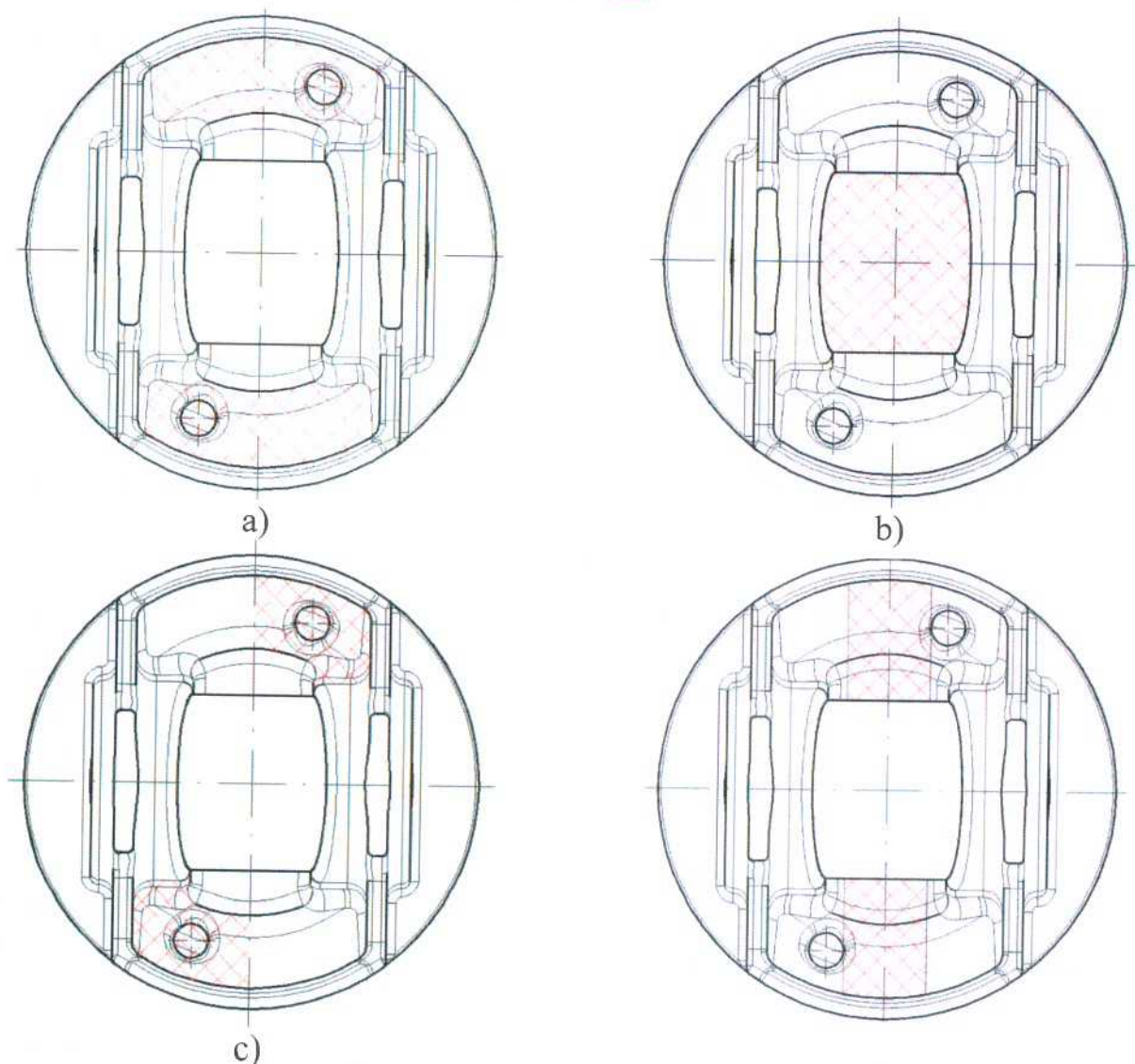


a)  b)  c)

Figure - 61. Restrictions of the undercrown area

On the other hand it is desirable to reach central part of the piston directly under the piston pin. In this simulation the nozzles will be mounted under the angle to cylinder axis. As an effect the impact point of jet on piston will drive from periphery to center from BDC to TDC (fig. 62).
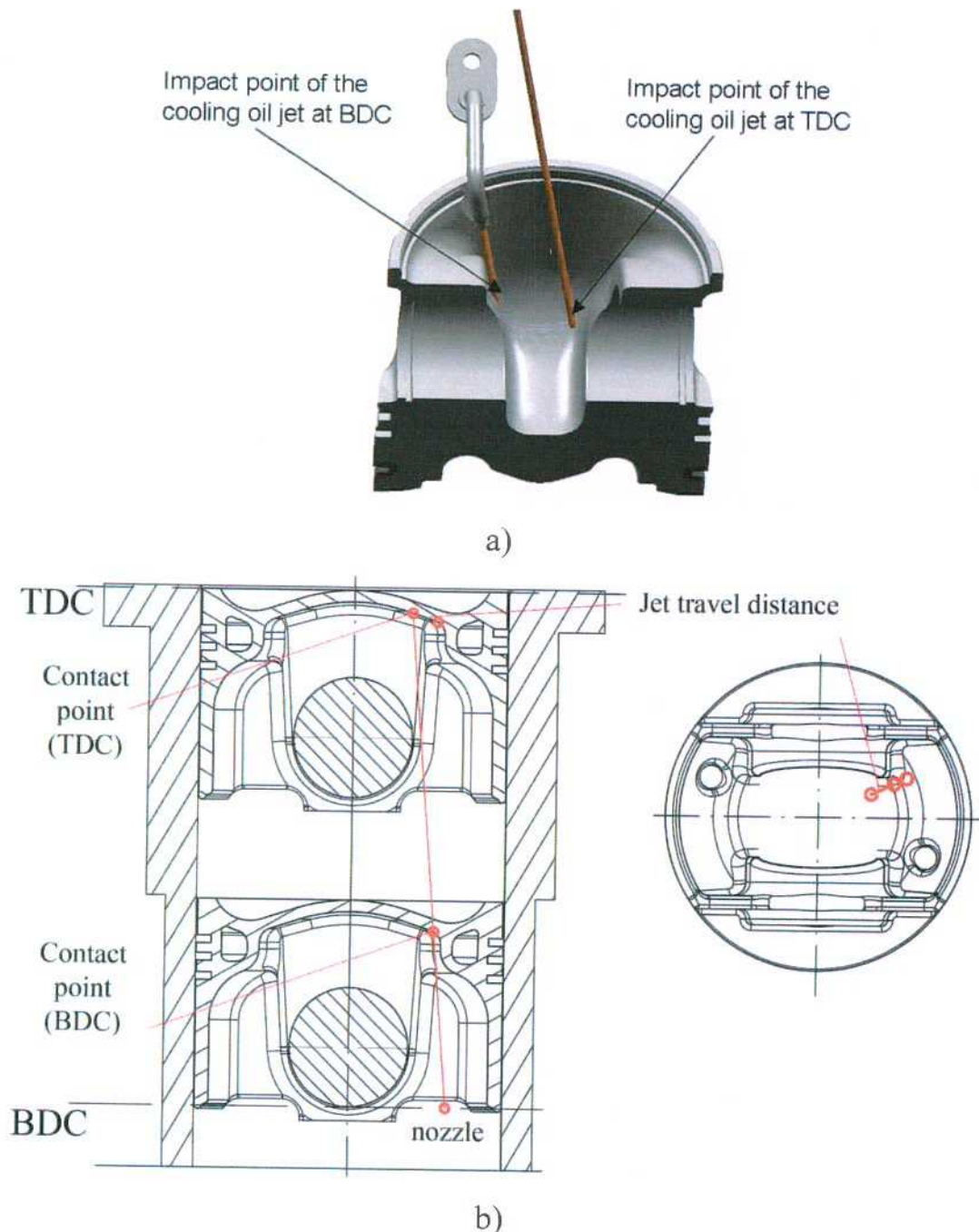


a)



b)

Figure - 62. Diesel piston with spray jet cooling of the undercrown: a) schema of the cooling process[5], b) A spray travel distance for the designed piston

Estimation of a heat transfer coefficient was made base on [23]. We could detach two zones (fig. 63):

- trace of the hydraulic jump (high intensity of heat transfer - $HTC_{jet} \approx 3000$ W/(m²K));

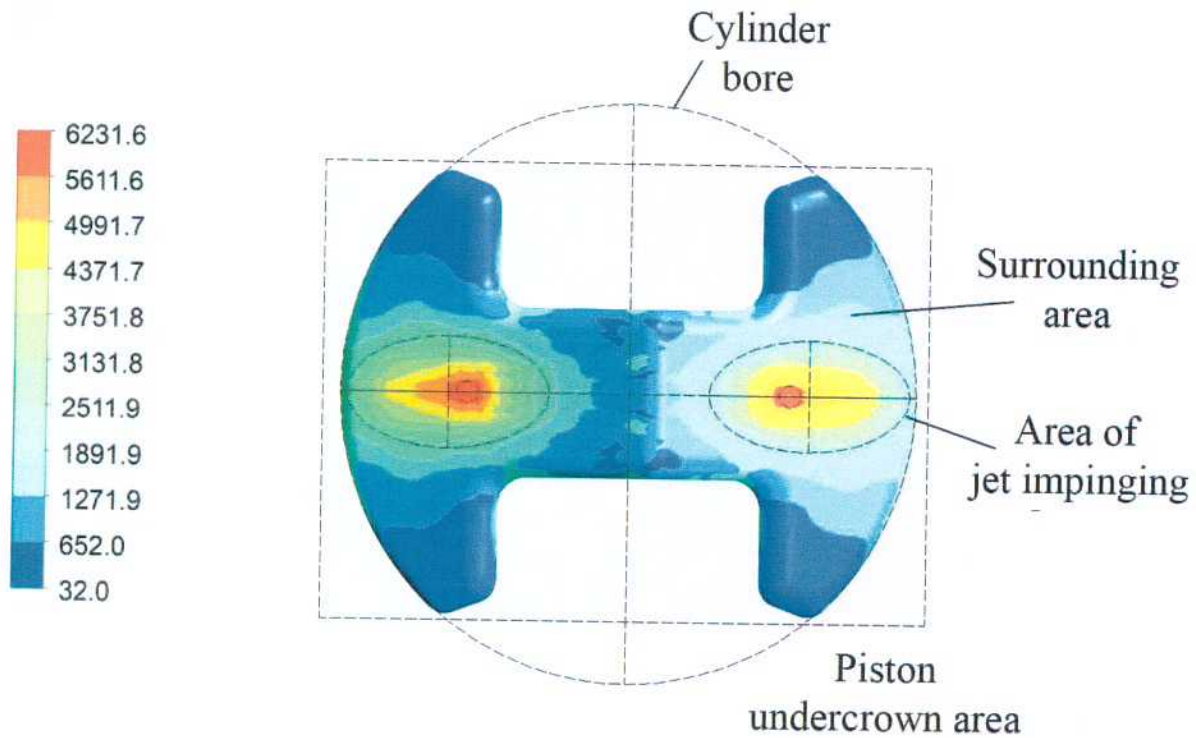- joined area (low intensity of heat transfer - $HTC_{jet} \approx 850$ W/(m²K)).



Figure - 63. Distribution of heat transfer coefficient in undercrown surface [5]

Indeed, the hydraulic jump radius is independent of the orientation of the surface (fig. 64). It means that oil is attached to piston surface in this area and it determines high intensity of heat transfer.
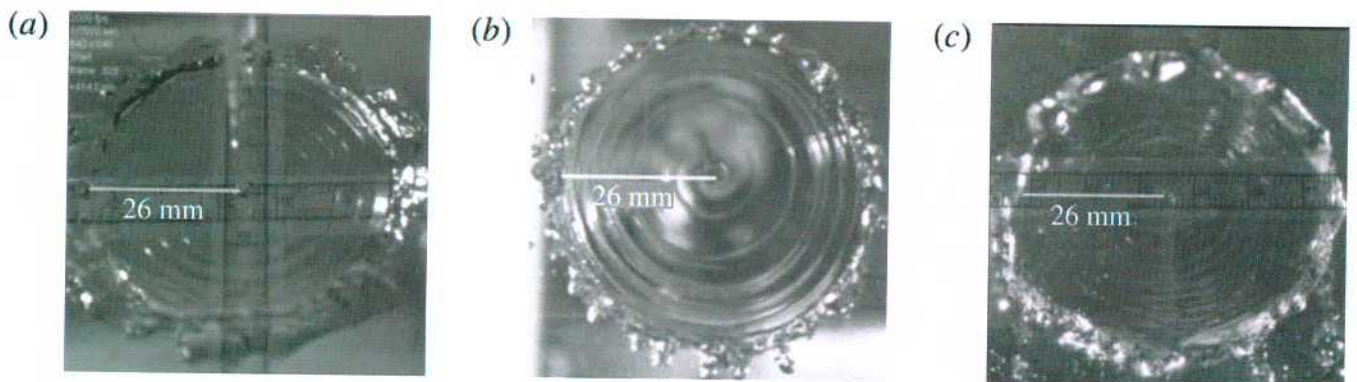


Figure - 64. Hydraulic jumps caused by a water jet impinging normally on surfaces: (a) Horizontal surface, (b) vertical surface, (c) horizontal surface [24]

The position of the hydraulic jump determines by correlation [25]:

$$r_0 = 0.0061 \cdot d_{inj} \cdot \text{Re}_d^{0.82},$$

(25)

here $\mathrm{Re}_d$ - jet Reynolds number and $d_{inj}$ - the injector diameter.
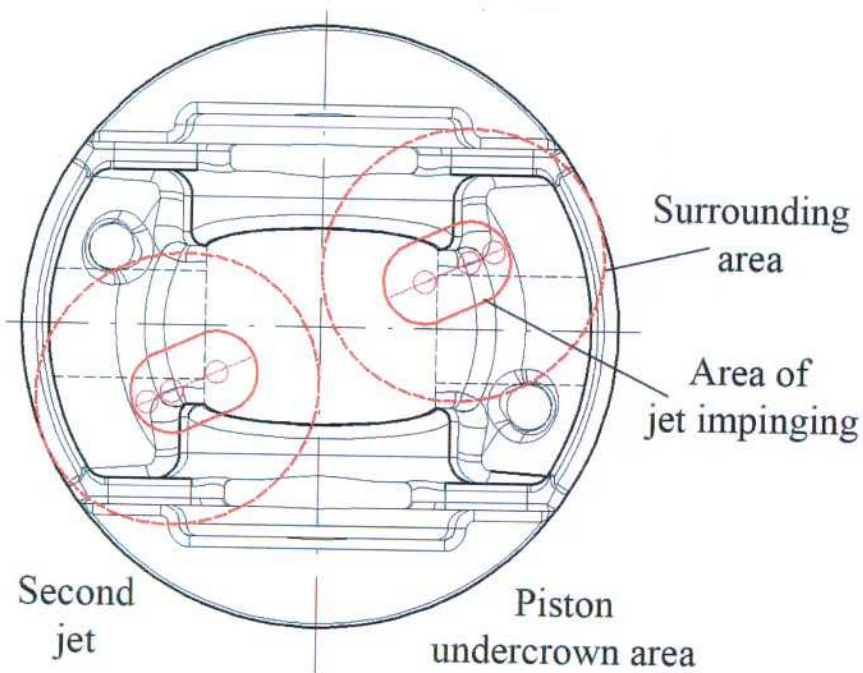
Finally the described zones are showed on fig. 65.



Figure - 65. Marked areas for the designed piston

The temperature field of the piston is shown on figure 66.

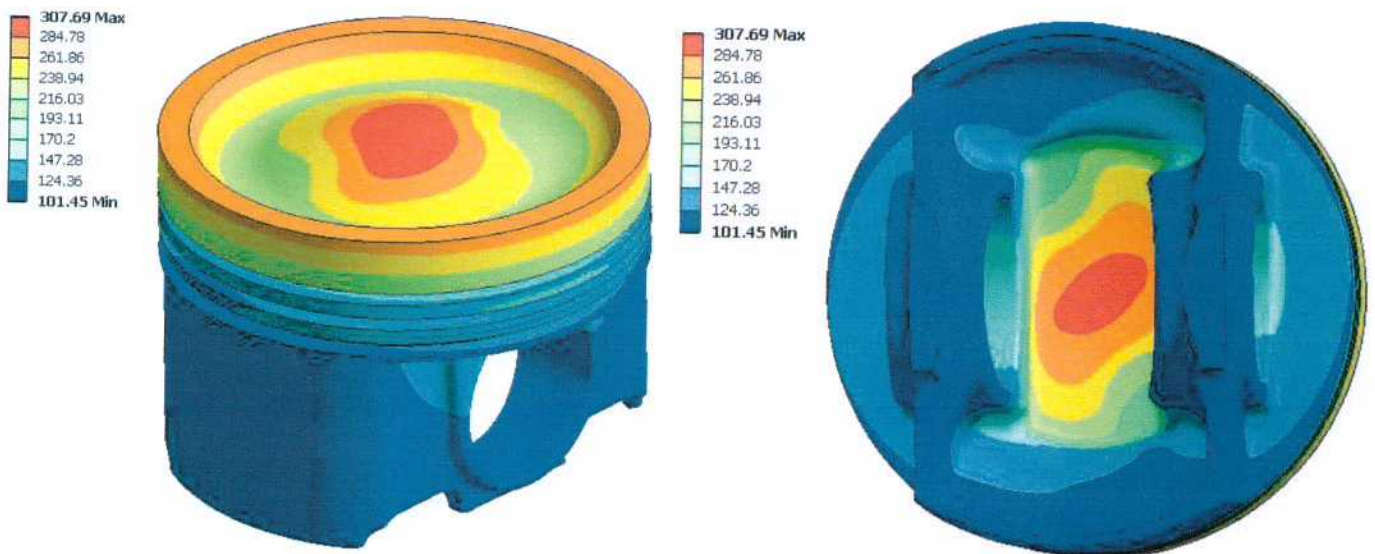The maximum combustion chamber temperature is 307 $^0$C. The maximum temperature in the ring belt zone is 227 $^0$C.



Figure - 66 Piston temperature

As it was mentioned there is no a big difference in ring belt temperature ($\sim 5^0$C) but the maximum temperature in the center of combustion chamber decreased at 81.5 $^0$C.

The difference in temperature dependent on type of cooling system is shown on figure 67.

Figure - 67 Temperature difference due to type of cooling system - combined and with cooling channels

## LITERATURE

1. Federal-Mogul Catalog 2017-2019, 916 p;

2. Kolbenschmidt Replacement Engine Parts Brochure 2019. 22p

3. Ottliczky, E.; et al.: Steel pistons for passenger car diesel engines. In: MTZ 72 (2011), No. 10, pp. 11–14

4. Hanke W, Ando H, Fahr M, Voigt M. Friction Reduction in Power Cylinder Systems for Passenger Car Diesel Engines. MTZ Worldw 2014;75:26–31. doi:10.1007/s38313-014-0018-y.

5. MAHLE GmbH (Ed)., " Pistons and Engine Testing ", Vieweg + Teubner, 2012

6. Maurizi M, Hrdina D. New MAHLE Steel Piston and Pin Coating System for Reduced TCO of CV Engines. SAE Int. J. Commer. Veh. 2016;9 (2):270 - 275

7. Richard Van Basshuysen, Fred Schafer Internal Combustion Engine Handbook: Basics, Components, Systems, and Perspectives. SAE 2004

8. H. Kajiwara, Y. Fujioka, and H. Negishi, Prediction of Temperatures on Pistons with Cooling Gallery in Diesel Engines using CFD Tool, SAE Technical Paper no. 2003-01-0986, 2003.

9. Kavtaradze R Z 2016 Local heat exchange in piston engines. Third edition (In Russian) (Moscow: Bauman State Technical University Publishing House) p 515

10. Takeshi Yoshikawa & Rolf D. Reitz (2009) Development of an Oil Gallery Cooling Model for Internal Combustion Engines Considering the Cocktail Shaker Effect, Numerical Heat Transfer, Part A: Applications: An International Journal of Computation and Methodology, 56:7, 563-578

11. H. Madarame, Den-netsu Kogaku Reidai Ensyu, Corona Publishing, Tokyo, 1991 (In Japanese). - *I have no ideas how to find this publication )))*

12. Chainov N.D., Ivashchenko N.A., Krasnokutskii A.N., Miagkov L.L. Konstruirovanie dvigatelei vnutrennego sgoraniia [Design of internal combustion engines]. Moscow, Mashinostroenie publ., 2011. 496 p.

13. Schommers, J., Lagemann, V., Böhm, J. et al. Steel Pistons for Mercedes-Benz PC Diesel Engines Lightweight, Efficient and Sustainable, MTZ Worldw (2015) 76: 4. https://doi.org/10.1007/s38313-015-0021-y

14. Hanke, W., Iijima, N., Müller, J. et al. MTZ Worldw (2019) 80: 18. https://doi.org/10.1007/s38313-018-0141-2

15. Hanke, W., Buschbeck, R., Letourneau, S., Sinclair, D. et al., "Power Cylinder System Friction and Weight Optimization in High Performance Gasoline Engines," SAE Technical Paper 2009-01-1958, 2009

16. Simon Gregor Schneider Mechanische und thermische Beanspruchungen in Großdieselmotoren bei extrem hohen Mitteldrücken Zugleich: Dissertation, München, Technische Universität München, 2012 LVK Lehrstuhl f. Verbrennungskraftmaschinen (2012), Deutsch, Hardcover ISBN 9783943813043

17. F. Szmytka, Mehdi Salem, Farhad Rezai-Aria, A. Oudin. Thermal fatigue analysis of automotive Diesel piston: Experimental procedure and numerical protocol. International Journal of Fatigue, Elsevier, 2015, 73, p.48-57.

18. Gabriel, D. and Hettich, T., "TopWeld® Steel Piston for High Speed Diesel Engines," SAE Technical Paper 2015-01-1723, 2015, doi:10.4271/2015-01-1723

19. Eder, T. et al.: Launch Of The New Engine Family At Mercedes-Benz. 24th Aachen Colloquium Automobile and Engine Technology, 2015

20. MAHLE GmbH (Ed)., "Cylinder components. Properties, applications, materials", Vieweg + Teubner, 2010

21. https://media.daimler.com/marsMediaSite/en/instance/ko/NANOSLIDE-Mirror-smooth-surface-for-less-friction.xhtml?oid=14316637

22. Richard Van Basshuysen, Fred Schaefer Audi AG, Fachhochschule Iserlohn "Internal Combustion Engine Handbook" 2004-12-06 SAE International

23. Mikhaylov, Yury V., Myagkov, Leonid L., and Malastowski, Nikolay S. "Numerical Simulation of Impinging Jet Cooling." *Proceedings of the 2010 14th International Heat Transfer Conference. 2010 14th International Heat Transfer Conference, Volume 5.* Washington, DC, USA. August 8–13, 2010. pp. 587-596. ASME. https://doi.org/10.1115/IHTC14-22654

24. R.K. Bhagat, N.K. Jha, P.F. Linden, D.I. Wilson, J. Fluid Mech. 851 (2018) R5.

25. Steven, J., Webb, B.W., 1989, Local Heat transfer Coefficients Under an Axisymmetric, Single-Phase Liquid Jet. Heat Transfer in Electronics -1989, ASME HTD-Vol. 111, pp. 113-119